Interacting tectonic faulting, karst subsidence, diapirism and continental sedimentation in Pleistocene deposits of the central Ebro Basin (Spain)

JOSÉ LUIS SIMÓN†, MARÍA ASUNCIÓN SORIANO, ANTONIO PÉREZ, ARÁNZAZU LUZÓN, ANDRÉS POCOVÍ & HÉCTOR GIL

Dpto Ciencias de la Tierra, Universidad de Zaragoza, 50009 Zaragoza, Spain

Abstract – During Early, as proposed by the International commission on stratigraphy Pleistocene times, interacting fluvial and aeolian processes constructed wide alluvial plains over an evaporite-dominated Miocene substratum in the central Ebro Basin. An exceptional site where these deposits show faults, folds, diapirs, karst structures and unconformities has been studied in detail. Analysis of particular structures demonstrates the interaction by that time of tectonic faulting, diapirism, karstification and sedimentation in an area where deformation was traditionally linked to the presence of underlying evaporites, without proposing any precise mechanism. Multiple approaches (sedimentology, structural geology and geophysics) have been used in order to discriminate the origin of each type of structure as well as to understand the interaction between different processes. Numerous normal faults and fractures of variable size are consistent with the regional stress field. Pleistocene deposits are pierced by diapirs of Miocene evaporites and disrupted by karst structures with different geometries (tubular, funnel and vault), both partially controlled by tectonics. The example described is proposed as an analogue model that could successfully illustrate evolution patterns of basins of potential interest for petroleum geology where similar processes have actuated, resulting in complex stratigraphical architectures.

Keywords: mantled karst, extensional tectonics, diapir, alluvial deposits, aeolian deposits, Pleistocene.

1. Introduction

1.a. Purpose of the study

Synsedimentary deformation in alluvial deposits has been widely studied around the world since it reflects distinct geological processes other than sedimentation. Different genetic mechanisms for deformation structures have been identified and interpreted both on a regional and a local scale: (i) tectonic structures *sensu stricto* generated by regional tectonic processes and consistent with regional stress fields (e.g. Blissenbach, 1954; Bull, 1968; Nemec & Steel, 1988; Mastalerz & Wojewoda, 1993); (ii) soft-sediment deformation structures produced by liquefaction mostly linked to propagation of seismic waves (e.g. Seilacher, 1969, 1984; Hempton & Dewey, 1983; Davies, Turner & Sansom, 2004; Gruszka & Loon, 2007); (iii) diapiric structures produced by migration of evaporites or plastic lutites (*mud diapirs*) (e.g. Morgan, Coleman & Gagliano, 1968; Simón & Soriano, 1986); (iv) karst subsidence structures, reflecting either slow sinking or a sudden collapse of sediments overlying karstified rocks (e.g. Soriano & Simón, 1995; Beck, 2004; Waltham, Bell & Culshaw, 2005; Gutiérrez, Guerrero & Lucha, 2008); and (v) ice wedge casts and other structures induced by periglacial processes (e.g. van

Vliet-Lanoë, Magyari & Meilliez, 2004; Briant *et al.* 2005).

Most research on this subject has generally focused on the study of individual geological processes; relatively few studies have been dedicated to understanding the relationship and interaction between different genetic types. The present paper aims to contribute to the literature on multiple relationships between faulting, karst subsidence, diapirism and sedimentation. Synsedimentary tectonic, karstic and diapiric structures affecting alluvial and aeolian deposits coexisted in the central Ebro Basin (Fig. 1a, b) during early Pleistocene time, resulting in a complex stratigraphical architecture. The main aim of this work is to discriminate between each intervening process and interpret how they interact by using geological and geophysical techniques. The results may be applied to other areas with similar deformational setting, either at similar or larger scales. The example described is proposed as an analogue model that could successfully illustrate evolution patterns of basins of potential interest for petroleum geology where similar processes have developed.

1.b. Background

A large number of studies carried out during the last decades have focused on diapiric and karstic deformations affecting the Quaternary alluvial deposits that overlie Early–Middle Miocene lutites and evaporites of
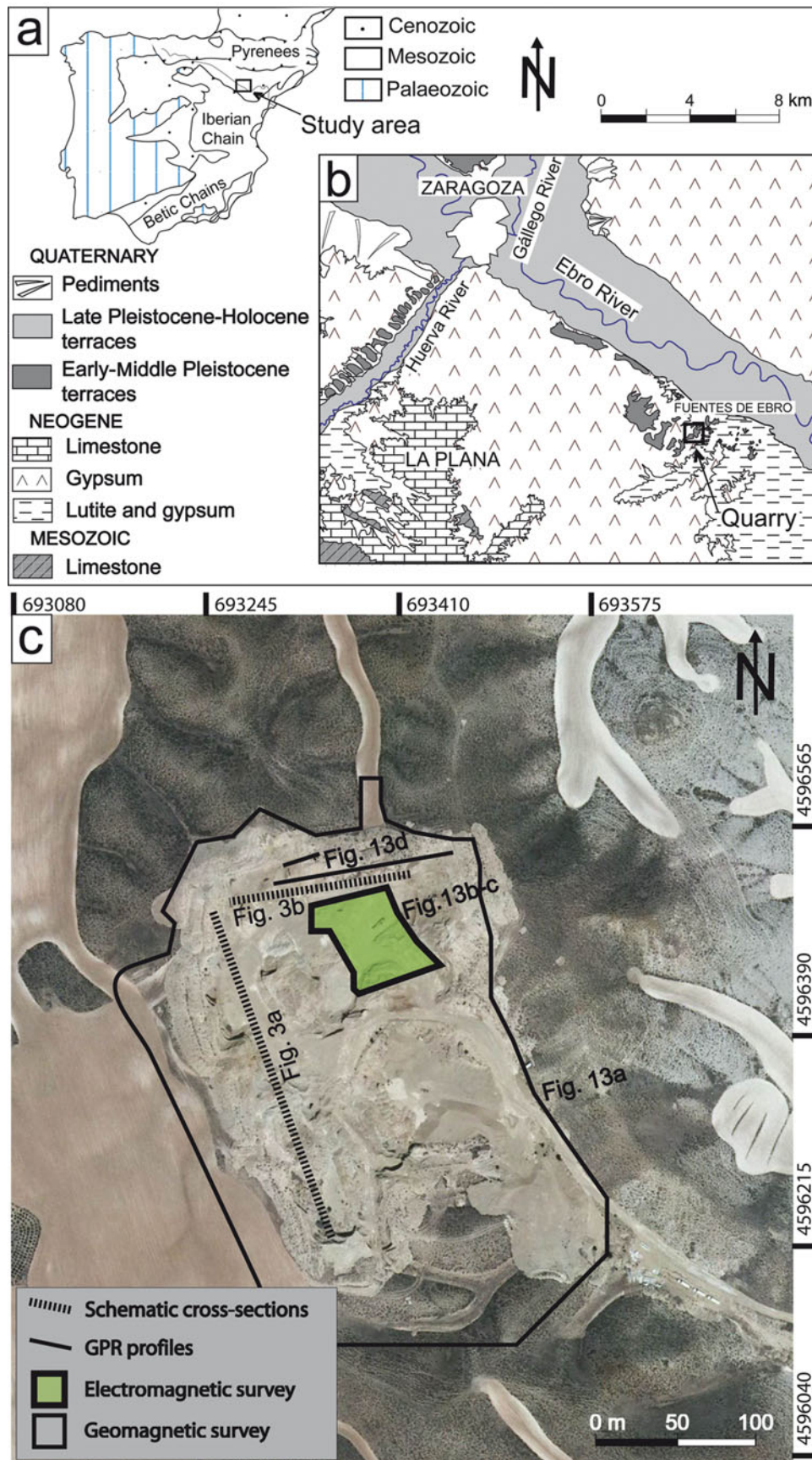
†Author for correspondence: jsimon@unizar.es

Figure 1. (Colour online) (a) Location of the study area in the Iberian Peninsula. (b) Geological map of the central Ebro Basin. (c) Aerial orthoimage (Instituto Geográfico Nacional, Spanish Government) showing the studied quarry in 2012, with location of cross-sections of Figure 3 and locations of geophysical surveys.

the central Ebro Basin. Simón & Soriano (1986) identified two types of diapiric structures (dome and piercing) affecting the oldest terraces of the Ebro River, the latter being associated with contractional structures (high-angle faults and monoclines). Benito & Casas (1987) described a third type (dome-piercing) in the Gállego and Ebro river terraces, developed during or very soon after deposition. Studies devoted to deformations associated with palaeokarst have allowed ductile synsedimentary structures to be characterized, as well as brittle postsedimentary structures developed in partially lithified sediments (Soriano & Simón, 1995; Benito *et al*. 1998; Gutiérrez, Guerrero & Lucha, 2008).

According to Simón & Soriano (1985, 1986), Benito *et al*. (1998), Soriano & Simón (1995) and Arlegui & Simón (2000) in the Ebro Basin, the following criteria can be used for distinguishing between tectonic, karstic and diapiric structures. (i) As karstic and diapiric structures are due to local vertical mass movement, they display cylindrical or conical 3D geometry with curved rupture patterns concentric with respect to the sinking or rising centre. (ii) Karstic and diapiric deformation usually only affects shallow levels, without any imprint on deeper rocks. (iii) Karstic and diapiric deformation structures usually have a significant ductile component and frequently result in loss of the original sedimentary textures and structures. (iv) Intrusive boundaries of piercing diapirs and karst–subsidence ruptures are represented by either normal, reverse or vertical contacts showing random strike. In contrast, tectonic faults show persistent orientations controlled by the regional stress field. In the case of the Ebro Basin, these are normal faults showing two preferred directions: one close to N–S (coherent with the regional extensional stress field) and another one to WNW–ESE (induced by inherited faults affecting the underlying Miocene rocks).

Little attention has been paid to understanding the relationships (and hypothetic interaction) between tectonic, diapiric and karstic deformation as well as between these processes and coeval sedimentation. Simón & Soriano (1986) provide examples of Quaternary diapirs locally triggered by tectonic normal faults in the central Ebro Basin. Benito & Casas (1987) suggest a relationship between diapiric structures and alluvial deposits thickened by karst subsidence: rapid loading in subsiding areas leads to high fluid pressure in fine-grained sediments and hence to gravitational instability and intrusion.

Such interactions have also been evidenced in other regions. Triggering of diapirs by faulting has been demonstrated by means of conceptual and analogue models (e.g. Vendeville & Jackson, 1992; Jackson, Vendeville & Schultz-Ela, 1994; Guglielmo, Jackson & Vendeville, 1997), as well as by regional studies (e.g. Pflug, 1973). Calaforra & Pulido-Bosch (1999) suggest that the presence of diapirs determines both the lithological and the hydrogeological setting at shallow levels, and hence the distribution and typology of large karstic forms in the Triassic lutites and evaporites

in the Betic Chains (Spain). Looff & Looff (2000) analysed the interaction between karst subsidence, piping and salt domes in the Gulf Coast, revealing that surface subsidence can occur above a shallow salt diapir due to the differential movement of the underlying salt. Further, extensional deformation of the strata overlying a salt diapir can produce a variety of fault patterns which in turn could control subsidence.

When occurring in an active sedimentary basin, these deformation types can interact with sedimentation. Synsedimentary unconformities (growth strata) are the major effects of local tectonics. They were first described at a basin scale by Riba (1976) and subsequently observed by other authors (e.g. Anadón *et al*. 1986; Muñoz & Casas, 1997; Aschoff & Schmitt, 2008). At a small scale, sediments deposited against a rising fold or fault are uplifted, deformed and eroded by continuous movement, occasionally drawing growth strata. These synsedimentary geometries have been described in relation to tectonic deformation (e.g. Miall, 1996), diapirism (e.g. Banham *et al*. 2011) or karst subsidence (e.g. Purdy, 1974; Gustavson, 1986; Ford, 1997; Dogan, 2005; Luzón *et al*. 2008; Silva *et al*. 2008).

2. Geological and geomorphological setting

The studied area is located in the central part of the Cenozoic Ebro Basin (NE Spain), *c.* 25 km ESE of Zaragoza city (Fig. 1b). This basin is bounded by the Pyrenees to the north, the Iberian Range to the south and the Catalonian Coastal Range to the east. In its central part, the thickness of the Palaeogene and Neogene series reaches 1500 m (Riba, Reguant & Villena, 1983). The Ebro Basin constitutes the last stage in the evolution of the southern foreland basin of the Pyrenees, and its general structure was achieved between the Late Oligocene and Early Miocene (Pardo *et al*. 2004).

By Late Eocene times, the connection between the Ebro Basin and the Atlantic Ocean was closed and the sedimentation became only continental. During this stage, alluvial fan systems (sourced in the three mountain ranges) and shallow evaporite and carbonate lacustrine systems developed (Muñoz *et al*. 2002; Pardo *et al*. 2004). Most of the exposed rocks correspond to terrigenous, evaporite (mainly gypsum and halite) and carbonate facies deposited in these sedimentary environments.

Endorheic sedimentation ended by Late Miocene times (12.5–8.5 Ma) as the Ebro Basin opened towards the Mediterranean Sea (García-Castellanos *et al*. 2003). A vast drainage system was established, eroding Miocene rocks while favouring Quaternary fluvial and alluvial sedimentation. Cold climate conditions during Pleistocene time favoured the development of proglacial alluvial plains in the Ebro Basin (Luzón *et al*. 2012). Glacial episodes were punctuated by warmer stages; such climatic fluctuations gave rise to a number of stepped terrace and pediment levels.

In the central sector of the Ebro Basin, Soriano (1990) recognized eight terrace levels mainly

developed in the right bank of the Ebro River (from the youngest, T1 to the oldest, T8). The recent terrace levels are well preserved and of kilometres in length, whereas remnants of variable size of the older terraces are only maintained on top of hills and mesas. The thickness of terraces falls within the range 5–25 m, although drills show local thicknesses in excess of 45 m (Guerrero, Gutiérrez & Lucha, 2004). The terrace deposits mainly comprise polygenic gravels with interbedded sands and silts. The gravels show horizontal bedding, cross-bedding (planar and trough) and clast imbrication. Scattered bands of Mn and Fe precipitates, as well as carbonate crusts at the top of the Quaternary deposits, appear frequently.

Stepped pediments (six levels; Soriano, 1990) are also identified in this area. The thickness of pediment deposits usually ranges from 1 to 6 m, although outcrops with 12 m of accumulated sediments have also been observed locally. Pediment deposits comprise sand, silt and angular to subangular gravel. Gravel structure is generally massive although horizontal bedding, imbricated clasts, low-angle cross-bedding and channel fill deposits have been recognized.

In general, the underlying Miocene beds are nearly horizontal or gently deformed by folds and faults (Quirantes, 1978; Arlegui & Simón, 2001). Tectonic deformation and stress fields in the central Ebro Basin during Neogene and Quaternary times were analysed by Arlegui & Simón (2000, 2001). According to these works, outcrop-scale faults and fractures within the Ebro Basin can be grouped into two main sets: (i) a N–S-striking older set developed under an intraplate stress field with S_{Hmax} oriented approximately N–S, related to forces caused by the convergence of Africa, Iberia and Europe and rifting at the Valencia trough; and (ii) a NW–SE- to E–W-striking younger set related to extensional deformation caused by differential isostatic movement at the Pyrenees and its foreland basin. A closer look at the first set shows that it is frequently split into NNW–SSE and NNE–SSW maxima. This is consistent with the recent to present-day tectonic setting of eastern Iberia, characterized by both spatial transition and time shifting between regional stress fields with NNW–SSE and NNE–SSW S_{Hmax} (Simón, 1989, 2006; Cortés et al. 1996; Andeweg et al. 1999; Herraiz et al. 2000). A detailed study of satellite images by Arlegui & Soriano (2003) shows that the aforementioned dominant directions are expressed on a regional scale as tectolineaments both in Miocene and Quaternary materials.

One of the most active geological processes in this region today is gypsum karst, represented by numerous alluvial dolines that cause frequent damage to urban areas (Soriano & Simón, 1995, 2002; Guerrero, Gutiérrez & Lucha, 2004; Pueyo-Anchuela et al. 2010; Soriano et al. 2012). Moreover, syn- and postsedimentary palaeodolines appear in quarries and trenches open in the Quaternary deposits (Luzón et al. 2008, 2011; Soriano et al. 2012). Locally, dissolution has caused strong aggradation of terraces and channel adjustments
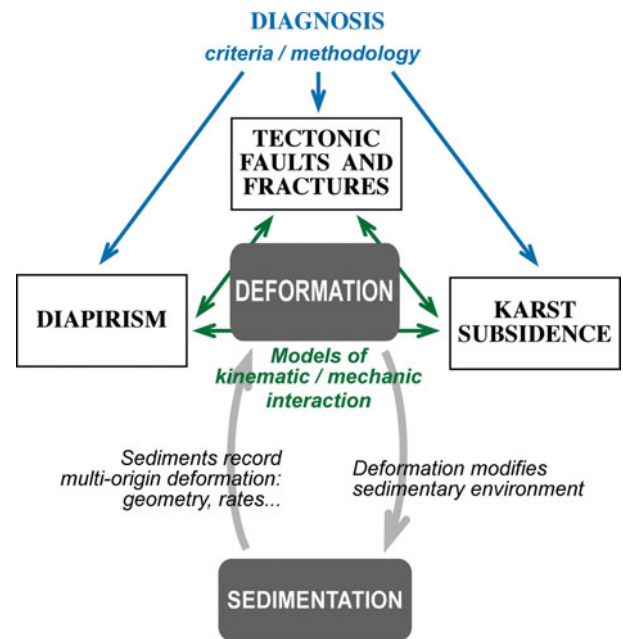

Figure 2. (Colour online) Conceptual and methodological scheme of the present study.

as in the oldest terraces of the Gállego River (Benito et al. 1998; Benito, Pérez-González & Machado, 2000).

3. Methodology

After intense fieldwork over the central Ebro valley, a large quarry was selected for detailed study (Fig. 1c). The criteria for quarry selection included good-quality, large-sized and diversely oriented exposures, as well as wide variety of facies and deformation structures. All these features allow a more complete view of the processes under investigation.

The general structure of the work is described by the logic tree of Figure 2. First, karstic, tectonic and diapiric structures need criteria to distinguish them as well as a common methodology for their structural analysis. Second, the interaction between and triggering of these structures should be explained by either kinematical or mechanical models. Finally, the complex sedimentary architecture is only understood from the interaction between deformation and sedimentation. Consequently, this study requires a multiproxy approach including diverse techniques as described in the following sections.

3.a. Geological analysis to characterize materials and structures

The sedimentological study aims to define, describe and interpret the main facies associations. Several lithofacies and architectural elements, in the sense of Miall (1978, 1996), have been defined in the area. Grain size analyses were made by dry sieving, using set-screens selected at 1/4 φ intervals. After being dried at 100 °C, the samples were put into a sieve tower and shaken for 20 minutes in an AMP0.40 W220 HZ59 device.
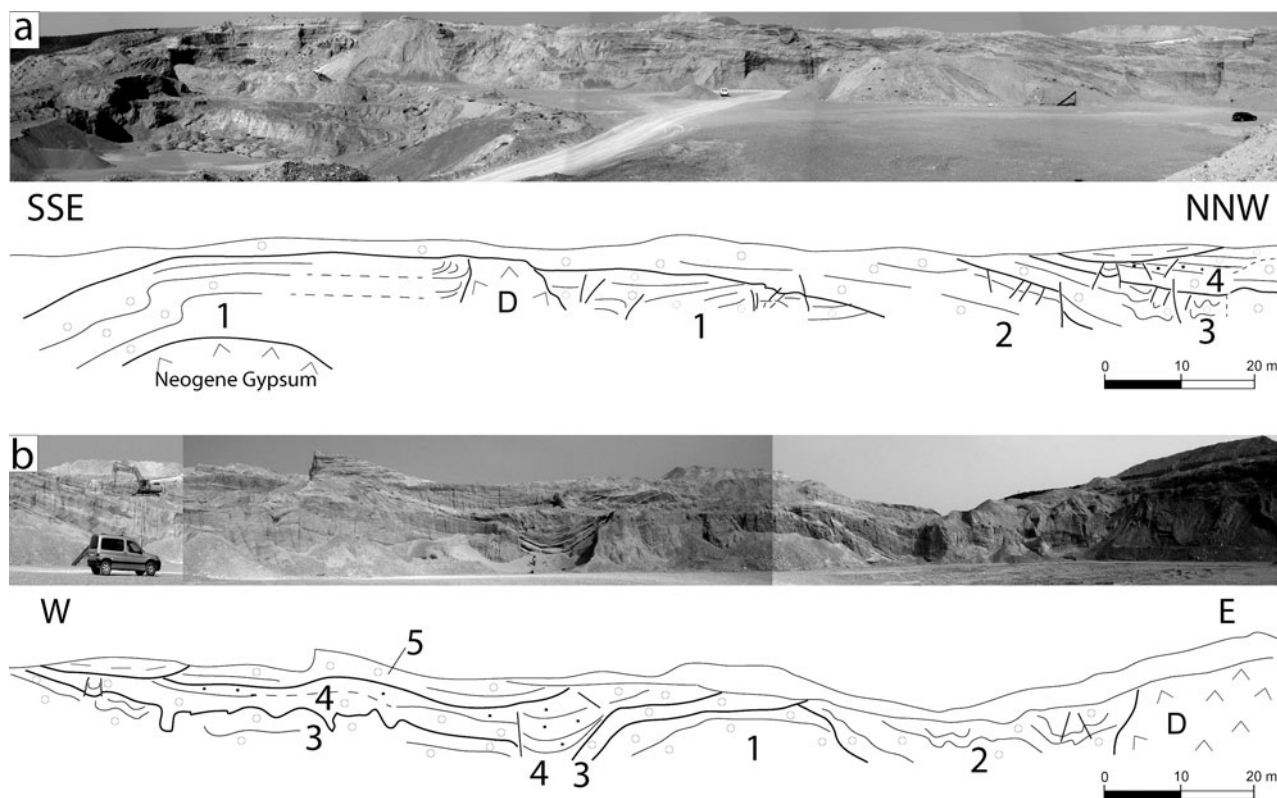
Figure 3. (a, b) Photographs and schematic cross-sections of the two main quarry faces (see location in Fig. 1c). 1, 2, 3, 4, 5: stratigraphic units; D: diapir.

Analysis of deformation structures (independently of their assumed origin) has followed a standard protocol based on exhaustive outcrop observation, elaboration of detailed cross-sections, measurement of displacements and the orientation of structural elements, projection onto equal-area stereoplots and kinematical reconstruction. The diagnostic interpretation of the origin of deformation structures has been based on the criteria listed above.

3.b. Geophysical analysis to approach the 3D geometry of deformation structures

A magnetometric survey (intensity and gradient of the magnetic field) was performed using two different devices: a proton magnetometer-gradiometer (PMG-01 from GF Instruments), taken as base for diurnal variation, and a magnetometer (GSM-19 from GEM-System) with GPS.

Electromagnetic radiation (EM) allowed measurement of the apparent conductivity and susceptibility of subsoil materials. Orthogonal profiles spaced 1 m apart were performed over the whole quarry floor, using a multifrequency electromagnetic sensor (GEM-02–163 device from GEM-System) with frequencies ranging from 330 Hz to 24 kHz.

A ground-penetrating radar (GPR) survey of the quarry floor (along profiles parallel to the main walls) and berms was made with a Ramac-GPR device provided with 50 and 100 MHz antennas.

4. Stratigraphy and sedimentology

A series of Pleistocene terrigenous deposits of thickness *c.* 60 m is exposed in the studied quarry. They belong to the oldest terrace of the Ebro River (T8 level according to Soriano, 1990) located at 210 m above the talweg. This terrace has been traditionally attributed to the Early Pleistocene based on its geomorphological position (Benito *et al.* 1998; Marqués *et al*. 1998; Colomer *et al.* 2006). A recent magnetostratigraphic study assigns it to the Matuyama chron, i.e. older than 773 ka (Gil *et al*. 2013*b*).

The stratigraphic series is strongly deformed, and internal angular unconformities are locally observed (Fig. 3). These discontinuities were the basis for defining five stratigraphic units. Faults affecting each unit are generally covered by the overlying unit. Broadly continuous (up to several metres) thick bodies of siliceous and carbonate gravels (mainly pebbles and cobbles) showing horizontal stratification predominate. Gravels are interbedded with mainly wedge-shaped sandy intervals that show a wide variety of sedimentary structures. Lutites are rarely present. The general stratigraphic succession of the studied outcrop is shown in Figure 4.

The sedimentological study of these deposits (Luzón *et al.* 2012) has revealed that water and wind processes interfered in an outwash plain where meltwater flow favoured gypsum dissolution and subsidence. Water-related facies associations are mainly longitudinal gravel bars, while dune sands and sandsheets are the most typical aeolian deposits.
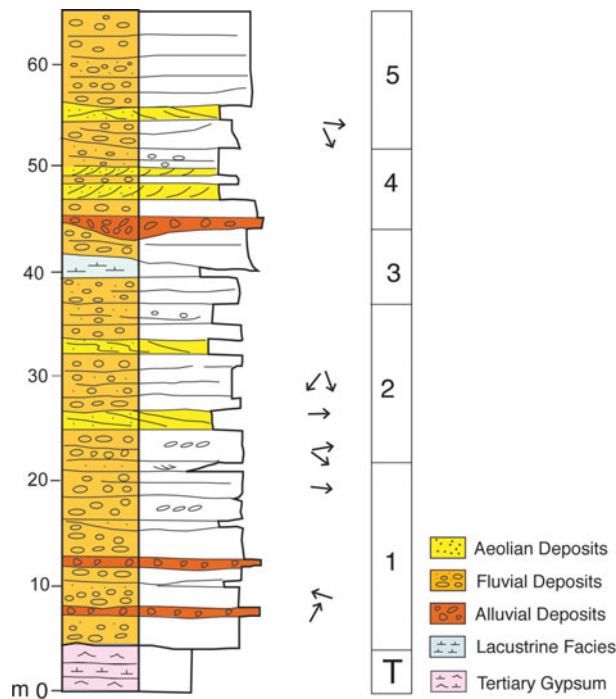
Figure 4. (Colour online) General stratigraphic sequence.

4.a. Architectural elements

4.a.1. Longitudinal gravel bars

These are represented by wide tabular bodies of gravels up to 3 m thick limited by planar or slightly irregular erosive surfaces. Interbedded wedge-shaped or lenticular sandy intervals are locally present. Grain-supported gravels show crude horizontal bedding due to textural changes (Fig. 5a, b). Well-sorted, rounded to subrounded siliceous and carbonate pebbles and cobbles derived from both the Iberian and the Pyrenean ranges predominate, but angular to subangular carbonate cobbles and boulders are also locally present (Fig. 5c). The latter are clearly derived from reliefs of Tertiary rocks close to the study zone. Imbrication is a common feature. Interbedded medium- to fine-grained sand levels are up to 40 cm in thickness and show horizontal lamination and rare cross-lamination. If present, they constitute the upper part of fining-upwards cycles. Gravel deposits represent tractive processes and the development of longitudinal bars in shallow gravel-bed braided channels, where conditions of rapid gravel transport favoured low-relief bars (Hein & Walker, 1977; Rust, 1978; Miall, 1978, 1996; Steel & Thompson, 1983; Shukla, 2009; Soreghan et al. 2009). Upward-fining cycles reflect bar accretion during waning discharges or lateral migration of channel ward-dipping bar margins (Smith, 1974; Miall, 1996).

4.a.2. Aeolian dune sands

These form up to 2 m thick lenticular to tabular intervals of fine-grained and very-well-sorted sands encased in gravels (Fig. 5d). Medium- to large-scale laterally continuous foresets (dipping near 30º) predom-

inate (Fig. 5e). Grain size data demonstrate that the saltation population (the steep central part of the cumulative frequency grain size curves; Visher, 1969) dominates, showing a good sorting as is common for aeolian sands (Folk, 1966). These grain sizes (mean grain size range 1.6–2.7φ; average 2.21φ) agree with the average grain size of aeolian dune sands (Lancaster, 1981, 1986; Mountney & Russell 2009; Rodríguez-López et al. 2006). These deposits are interpreted as aeolian dunes with a well-developed slipface on the lee side (Kocurek, 1991; Scherer, 2000), indicating that dune crests were mainly transverse to the wind direction.

4.a.3. Aeolian sandsheets

They are represented by decimetre-thick laterally continuous tabular strata of fine-grained very-well-sorted sands (Fig. 5f). These strata are in turn organized in tabular sets that show pinstripe lamination, a very common feature of wind-rippled deposits (Fryberger and Schenk, 1988; Mountney, 2006b). The described sedimentary bodies represent aeolian sandsheets formed by the vertical accumulation of subcritically climbing translatent wind ripples (Hunter, 1977, 1981; Kocurek & Dott, 1981; Mountney et al. 1999; Veiga, Spalletti & Flint, 2002; Mountney, 2006a).

4.a.4. Hyperconcentrated flow deposits

These consist of massive gravels with plentiful sandy matrix (Fig. 5g). Clasts are rounded to subrounded and locally imbricated. Sandy matrix is very well sorted and has similar mean size as the described aeolian sands. These features suggest hyperconcentrated flows characterized by rapid deposition under high discharge conditions (Smith, 1986). Sandy matrix is interpreted as derived from water reworking of aeolian sand dunes leading to an admixture of sand into the fluvial channels.

4.a.5. Shallow lake deposits

Rhythmically laminated (visible from colour variations) or massive clay-dominated deposits, up to 2 m thick, represent the less-abundant lithology in the studied area (Fig. 5h). Oxidized plant remains and bioturbation are occasionally recognized. These sediments are interpreted as deposited in ponds or small shallow lakes.

4.b. A special sandy deposit

A thick, mainly sandy U-shaped fill located in sectors 4 and 5 constitutes a striking feature within the studied quarry (Fig. 6). This deposit corresponds to unit 3 in the stratigraphic log of Figure 3b. It corresponds to a deformed detrital succession trapped in a subsiding domain, c. 10 m wide and at least 7 m thick. Its western margin is represented by a nearly
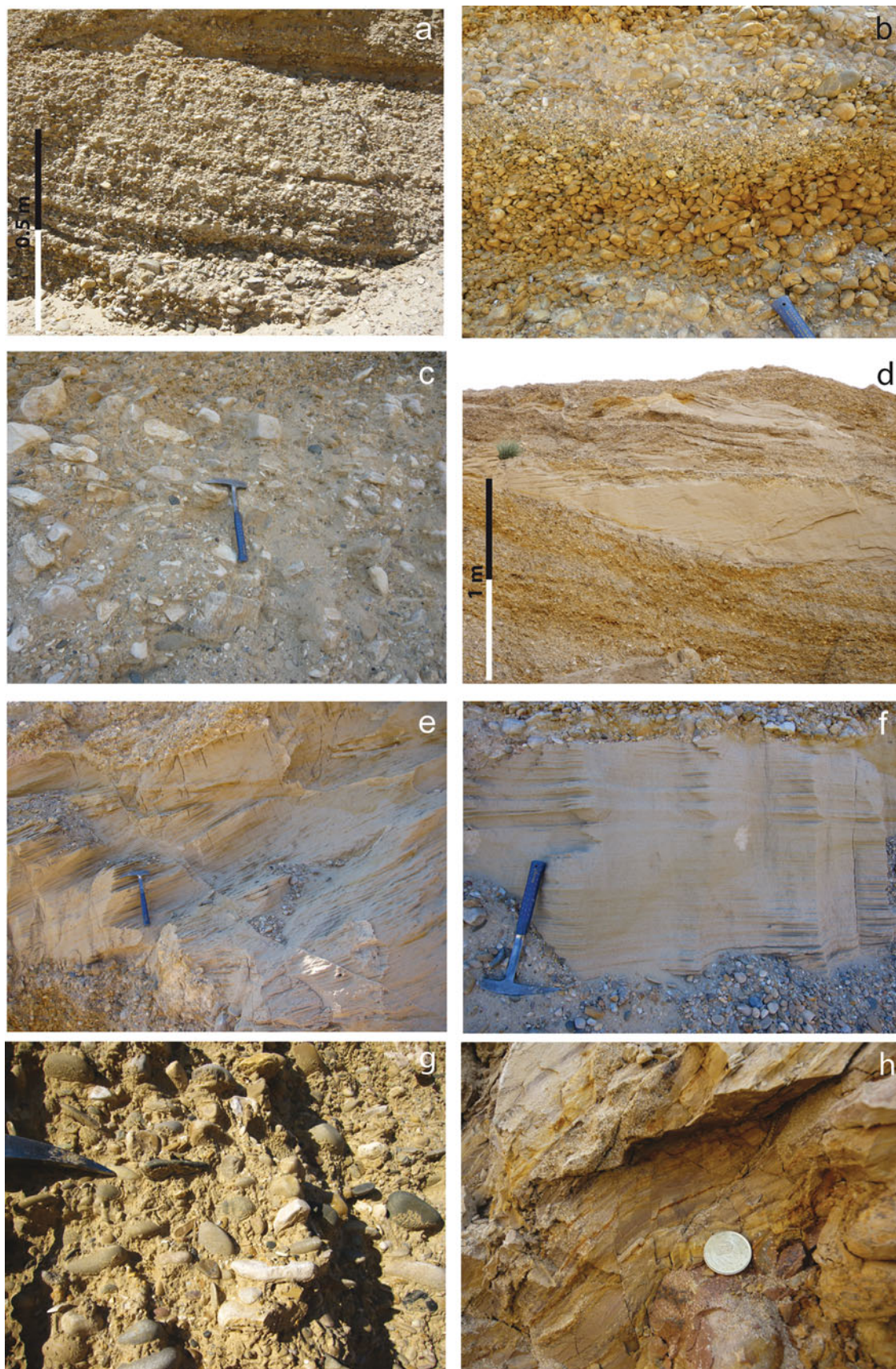
Figure 5. (Colour online) (a, b) Longitudinal gravel bars. They are mainly integrated by well-sorted rounded to subrounded siliceous and carbonate pebbles and cobbles. (a) Horizontal stratification, mainly due to textural changes, characterizing the longitudinal gravel bars. (b) Differences in the sandy matrix content between gravel beds are very common. (c) Locally angular to subangular carbonate cobbles and boulders are also locally present. (d) Transverse aeolian dune encased in fluvial gravels. (e) Close view of an aeolian dune sand foreset. (f) Close view of an aeolian dune sandsheet encased in fluvial gravels. (g) Hyperconcentrated flow deposits. Sandy matrix is very well sorted and has similar mean size as the aeolian sands. (h) Laminated lacustrine deposits. Lamination is related to either colour changes, as in figure, or grain size variations.
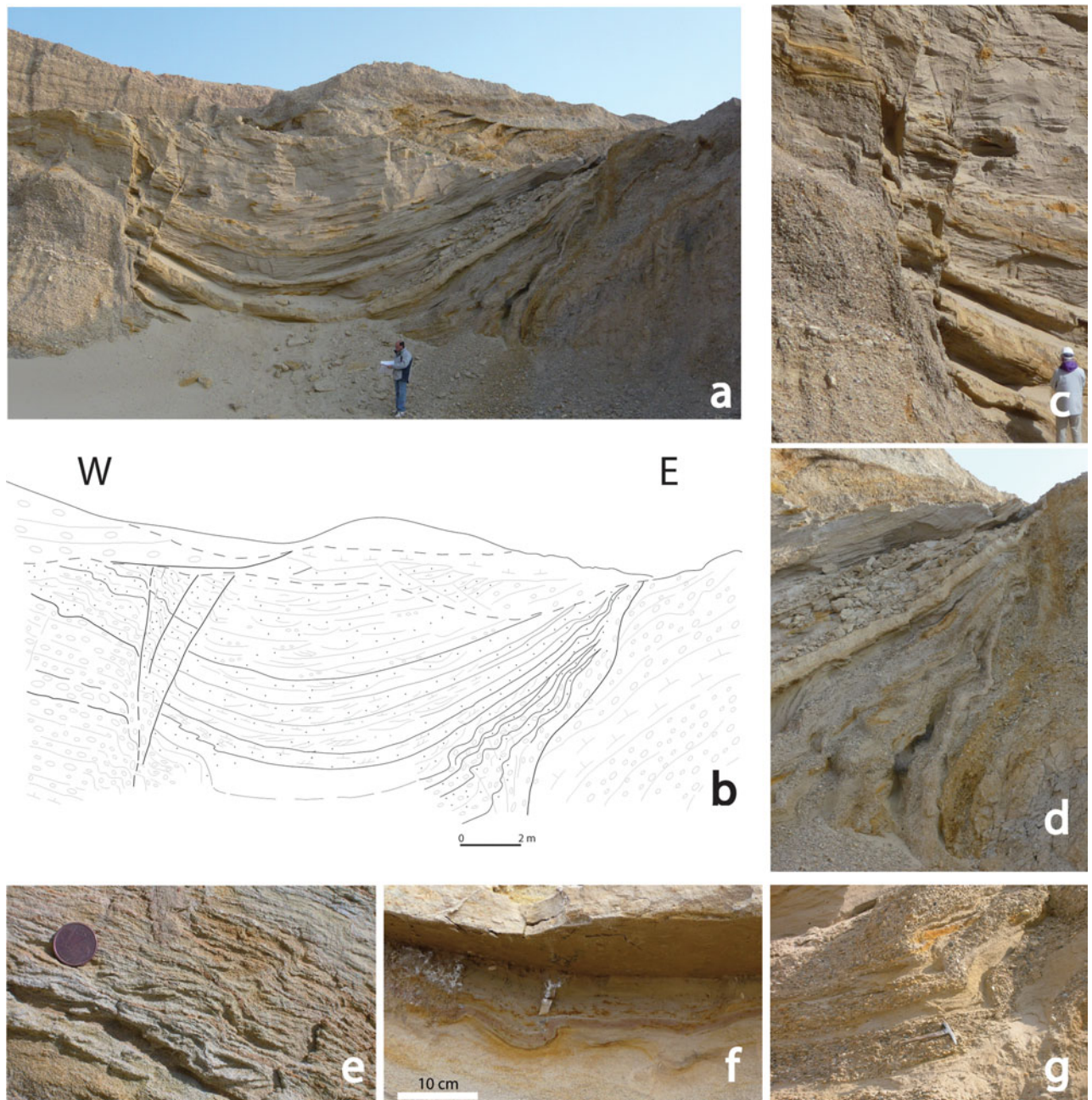
Figure 6. (Colour online) Sandy, U-shaped fill in sectors 4–5 (see location in Fig. 9). (a) Field view. (b) Cross-section. (c) Detailed photograph of faults at the western border. (d) Growth strata at the eastern border. (e) Reverse faults and folds at the western limb. (f) Soft-sediment structures in the central area. (g) Asymmetric folding of gravel beds at the eastern limb.

vertical fault zone; the eastern margin is represented by growth strata recording synsedimentary subsidence. The occurrence of soft-sediment deformation structures (mainly convolute lamination) affecting sand layers close to the margin corroborates this interpretation. The main features of the sedimentary fill are represented in Figure 6b. Gravels are present in the base of the series, but sands do predominate. Decimetre-thick cross-strata sets of aeolian sands dominate in the middle part, while water-reworked aeolian sands, organized in superimposed mega-ripple cross-strata with small floating pebbles, become dominant towards the top. Deflation lags between aeolian and water-reworked aeolian deposits suggest alternating periods of wind

erosion, wind deposition and flooding events. Occasional centimetre-thick lutite layers with mud cracks, mainly interbedded between the aeolian sands, suggest ephemeral swamping. The overlying fluvial gravel bars are only slightly deformed and cover unconformably the described deposit, indicating the decrease of deformation with time.

4.c. Palaeogeographical sketch

The described lithofacies indicate that the palaeogeographical sketch in the area was dominated by a gravel braided fluvial system that mainly flowed towards the SE (Fig. 7). Even though source areas were mainly the
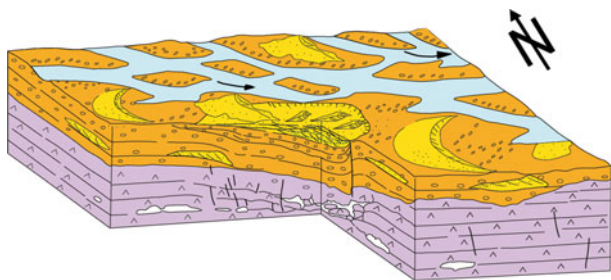
Figure 7. (Colour online) Three-dimensional diagram showing the sedimentary conditions that gave rise to the preserved sedimentary succession in the study region. Aeolian dunes developed over braided fluvial gravels. Dissolution cavities in the Miocene evaporites deformed fluvial beds due to synsedimentary subsidence and favoured the localized preservation of aeolian deposits.

Pyrenean and Iberian ranges, sedimentary supplies also came from close palaeoreliefs (as indicated by the recurrent subangular limestone boulders). Shallow channels and longitudinal bars mainly integrated the fluvial system. The stratigraphic architecture shows the interference of fluvial and wind processes. Aeolian forms migrated in the alluvial plain, probably during periods of low river discharges. Dunes moved mainly towards the east, in agreement with the present dominant wind direction in the region. High-energy flows reached the area during some stages, leading to dune destruction and generating hyperconcentrated flow deposits. Subsiding areas in the alluvial plain led to deposition of wind facies (due to wind deceleration) or settling out of lacustrine deposits. Fine-grained facies were preserved from subsequent erosion as subsidence placed them below the base level of erosion.

5. Structural study

The studied deposits show the imprint of conspicuous and intense, both brittle and ductile, deformation at centimetre to hectometre scale. Internal angular unconformities clearly demonstrate the synsedimentary character of structures at larger scales.

5.a. Description and analysis of deformation structures

Faults and fractures are pervasive over the whole quarry. Faults are mostly normal, and more frequently appear as N–S- to NNW–SSE-striking surfaces with a scale of the order 10^{-2} to 10^2 m, dipping both eastwards and westwards (see Figs 6, 8 and stereoplots in Fig. 9). They show variable (from negligible to metre-scale) vertical offsets. The measured dip separations are minimum at sectors 2, 3 and 4 (0.1–3 cm), become significant at sectors 6, 8, 11, 12 and 13 (10–70 cm) and attain maximum values at sectors 5 (3 m) and 14 (2 m). Fractures appear at decimetre to decametre scale, dipping both eastwards and westwards and showing from negligible up to metre-scale vertical offsets. Several collected samples of minor faults and fractures make conjugate systems compatible with stress ellips-

oids characterized by a nearly vertical σ_1 axis, a nearly horizontal N–S to NNW–SSE σ_2 axis and a nearly horizontal E–W to ENE–WSW σ_3 axis.

Large normal faults with offsets up to 1–2 m appear at sectors 7 and 14, where they are the only deformation structures. They show N–S, NW–SE and W–E directions and cut nearly horizontal fluvial beds, without any relationship to either folds or reverse faults.

In contrast, the most conspicuous fault in sector 5 is a part of the complex 'negative' structure whose sedimentary infill is described in Section 4.b. It is a nearly vertical, NNW–SSE-striking fault that comprises the western boundary of a synform whose visible section is *c.* 10 m wide and 7 m high (Fig. 6a, b). This synform has an axis gently plunging towards the NNE (Fig. 9, stereoplot 4B) and limbs dipping up to 40º NE and 60º NW, respectively. Several high-angle, reverse, west-dipping faults splay out from the main fault surface (Fig. 6c), showing similar strike to the former (see stereoplot corresponding to sector 5 in Fig. 9). The eastern margin (sector 4 in Fig. 9) comprises a growth strata structure that evinces synsedimentary subsidence (Fig. 6d). In addition, numerous micro- and meso-scale reverse faults (showing offsets from 2 mm to 20 cm) deform both limbs of the syncline (Fig. 6e, f). Most of these are actually ductile structures (small associated propagation folds showing kink morphology) in which the continuity of the sedimentary layers has not been interrupted. Both micro-fault surfaces and axial surfaces of propagation folds mainly strike NNW–SSE close to the western boundary, whereas they show very variable orientation at the eastern boundary (see stereoplot corresponding to sector 4 in Fig. 9). Finally, a number of soft-sediment deformation structures affecting fine clastic levels (Fig. 6g) appear within this structure, suggesting the occurrence of liquefaction processes. Considering their sedimentary and deformational framework, these could be triggered by either sudden karst collapse or tectonic faulting events.

Other example of negative structure bounded by reverse-limb monoclines ('vault' morphology) is located at sector 9 (Fig. 10a). It appears as a narrow (3.5 m) box-shaped syncline deforming unit 2, with oblique limbs that converge and apparently close the structure to the west.

The rest of the ductile deformation structures observed in the quarry are linked to limbs of two prominent bodies (of Miocene marls and gypsums) cropping out at sectors 2 and 13–14. They constitute the cores of positive structures in which the Quaternary cover has been partially pierced. The visible thickness of the alluvial deposits drastically diminishes from *c.* 30 m to less than 2 m at the crest. At contacts between Miocene and Pleistocene materials, proofs of differential vertical movement, such as sharp monoclines, intrusive boundaries and gravel–marl melanges, are found. The western visible limb of the structure cropping out at sector 2 shows a dominant NNW–SSE strike, that is, parallel to the prevailing faults. The emplacement of such bodies has induced internal deformation in gravels and sands
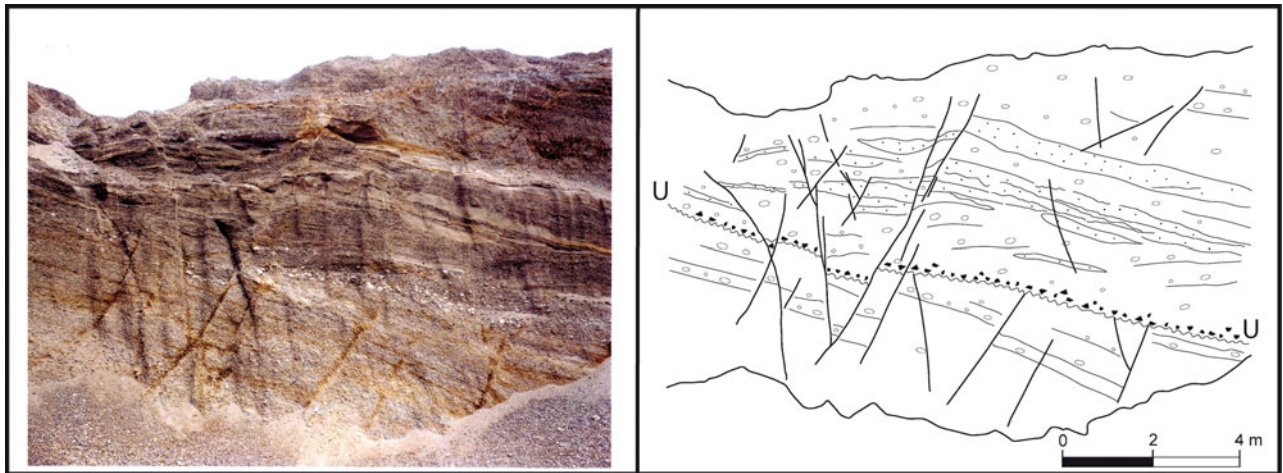
Figure 8. (Colour online) Normal fault system in sector 6 (see location in Fig. 9). Note that some faults are previous to the unconformity (U), while others affect the entire sedimentary series.

at distances of up to several tens of metres from their boundaries. Typical deformation structures are reverse kink-bands affecting gravel and sand beds (showing only a moderately angular geometry due to the coarse grain of sediments). Conspicuous examples are found at sector 2, close to the above mentioned western limb (Fig. 11). The amplitude of each individual fold is usually of decimetre scale and the strike of axial planes is also NNW–SSE. Although the majority of kink-bands dip towards the marl-and-gypsum body, conjugate west-dipping kink-bands also appear. During the last stage of this study, mining works within the quarry revealed two new minor intrusive structures in sector 13. Both produce conspicuous deformation of Pleistocene sands and gravels, although one of them does not show Miocene materials cropping out at its core.

Finally, tubular and funnel structures disrupt the Pleistocene sediments, cutting them either vertically or obliquely (Fig. 10b). These are also filled with Pleistocene gravel and sand beds, frequently accommodated in the walls of the structure (pebbles close to the walls have their major A-axes vertical or nearly vertical). The rest of the infill is either unstructured or shows interbedded gravels and sands.

5.b. Genetic interpretation of deformation structures

Frequently, discriminating the genesis of deformation structures in Pleistocene deposits of the central Ebro Basin is not an easy task. In the past, there was a tendency to attribute every anomaly to the effect of the underlying Miocene evaporites, without proposing any explicit deformation mechanism. Indeed, suballuvial dissolution of gypsum and other evaporitic deposits induces strong deformation of the Pleistocene cover, giving rise to deformational contacts and strong local thickening of alluvial deposits (Benito et al. 1998). Further, diapiric processes (either halokinesis of evaporites, or plastic flow of water-saturated lutites as occurs in mud diapirism defined by Morgan, Coleman & Gagliano, 1968) generate dome or antiform struc-

tures with their core frequently pierced by the intrusive materials (Simón & Soriano, 1986; Benito & Casas, 1987). Nevertheless, many other structures should be related to regional tectonic deformation, that is, to regional stress fields linked to the prevailing geodynamic mechanisms at the NE Iberian plate during Neogene–Quaternary times: (i) Europe–Iberia–Africa convergence; (ii) rifting at the Valencia trough; and (iii) residual and topographical body forces at the Pyrenean Orogen (Liesa & Simón, 2009). Stress systems resulting from such tectonic settings are mostly extensional (vertical σ_1 axis), with nearly horizontal E–W to ENE–WSW σ_3 axis (Simón, 1989; Andeweg et al. 1999; Herraiz et al. 2000).

In the studied quarry many normal faults and fractures comprise conjugate systems with persistent N–S to NNW–SSE strikes that are fully compatible with the regional stress field. Most large normal faults, although not comprising visible conjugate systems, are also oriented close to N–S. On the basis of these features we interpret a tectonic origin for these faults.

The positive structures showing a Miocene core that pierces the Pleistocene cover are interpreted as diapirs. Such deformation structures, developed at the metre to decametre scale, are common within fluvial and alluvial deposits all over the central Ebro Basin (Rioja, south Navarra and Zaragoza sectors). Diapir growth has mainly induced contractive internal deformation in the Pleistocene unconsolidated gravels and sands, up to 15–20 m from their boundaries. Combined rising and wedging effects related to the intrusion involve horizontal shortening that produces typical high-angle reverse faults and contractional kink-bands with pebbles rotated and frequently striated (Simón & Soriano, 1986; Benito & Casas, 1987).

The tubular, funnel and vault structures that disrupt the Pleistocene detrital deposits are interpreted as being related to karst processes at depth. Funnel structures represent the uppermost expression of subsidence. Tubes are intra-alluvial conducts connecting surficial collapses with cavities in the underlying
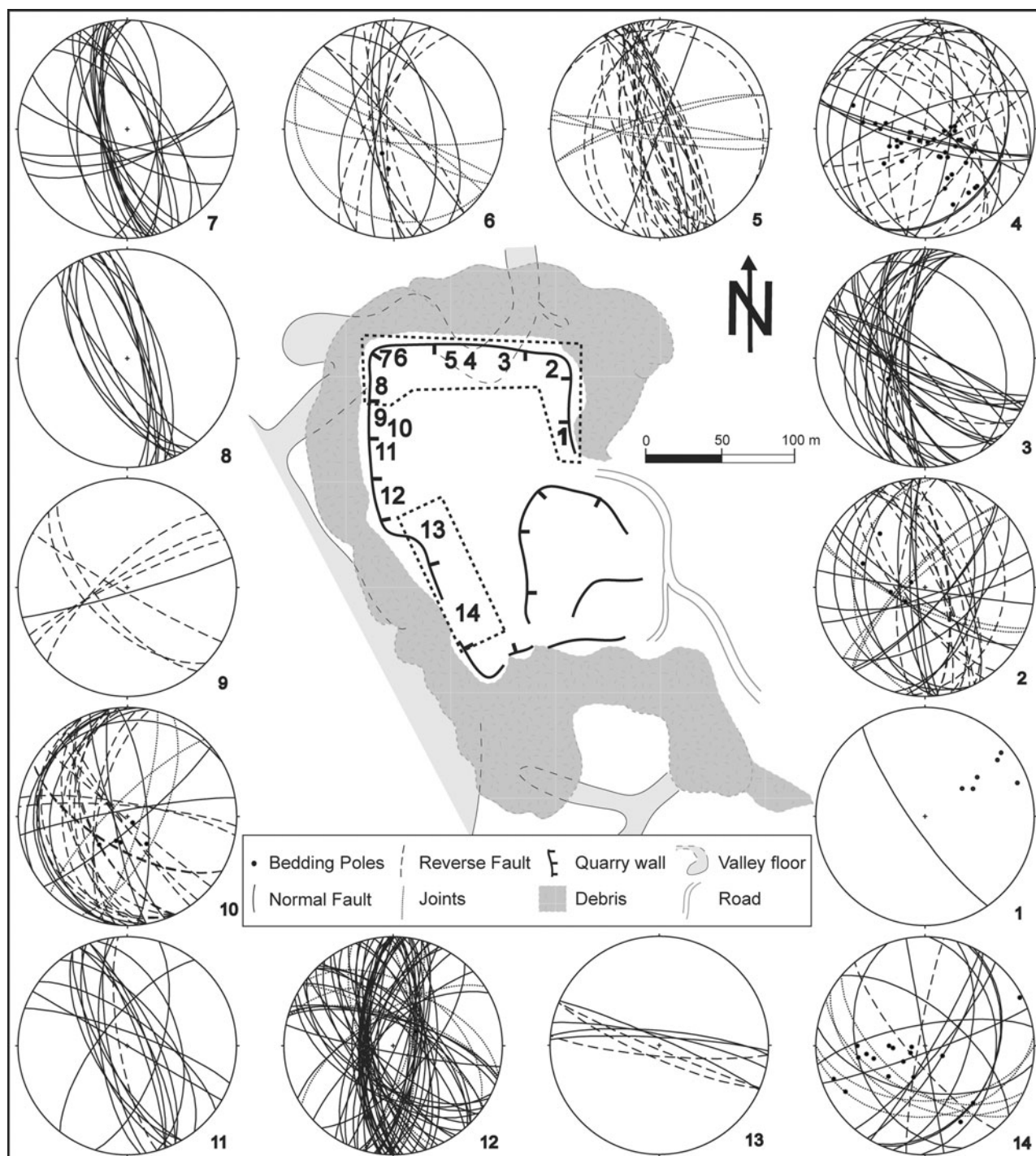
Figure 9. Structural data from the studied quarry: schematic plan view (position of quarry walls in June 2010) and stereoplots of bedding and fracture orientations collected along the different sectors.

Miocene evaporites. Vault structures are mostly related to upwards propagation of cavities in cohesive materials. Such propagation is due to the development of successive downwards-concave tensile fractures controlled by the lithostatic stress trajectories ('tension dome') above the cave (Ford & Williams, 1989).

The negative structure outcropping at sectors 4–5 described in Section 4.b also has some features of karstic subsidence structures, that is, curved rupture surfaces and significant ductile deformation. In our opinion, this structure could constitute the most conspicuous

and expressive example. Nevertheless, this has clear tectonic control since a nearly vertical N–S-oriented fault forms its western boundary. Unfortunately, outcrop conditions did not allow us to assess whether the 3D geometry corresponds to either a cylindrical or an elongated N–S-trending sinking body. For this reason, a geophysical survey was achieved in order to discern its tectonic or karstic origin.

The characteristics of this deformation structure probably evince a rheological behaviour of the alluvial cover which can be described as between cohesive
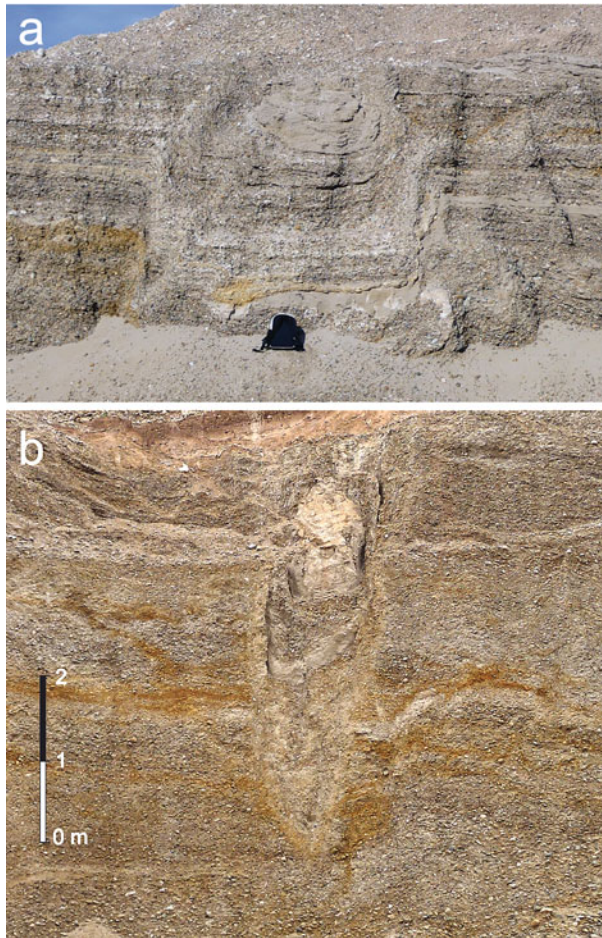
Figure 10. (Colour online) (a) Metre-scale collapse structure with vault morphology in sector 8 (see Fig. 9). (b) Oblique section of a metre-scale tubular structure in sector 7.

and non-cohesive. In the former, alluvium is dragged down into pipes opened in the underlying evaporites. The sinking material behaves as a fluid, losing its original texture and filling voids in the subsoil. The process resembles the operation of a sandglass. In the latter case, cavities developed in the soluble substratum are maintained wide for some time, but tensile failure and disengagement of successive concentric slabs from the ceiling finally result in sudden collapse of the clastic cover. The sinking body, although possibly broken into blocks, tends to maintain its internal texture and is separated from the non-deformed beds by brittle, frequently open vault-shaped fractures (Soriano & Simón, 1995).

The detrital deposits in the synform have maintained their integrity (layers are continuous from one limb to the other one), and most 'reverse' structures are not brittle cracks but reverse kink-bands or sharp monoclines. These involve net horizontal shortening of the sinking layers, which does not occur in the case of collapsed vault-shaped structures. A simple kinematical model (Fig. 12) describes the evolution of the synform. Consider a non-cohesive alluvial cover (I) in which a funnel-shaped body, bounded by non-disrupted material, flows into a karstic tube losing its internal structure

according to the 'sandglass' model (II). Then suppose that new sedimentary material with some degree of cohesion fills the surficial depression (III), before undergoing renewed subsidence as the underlying material is removed (IV). This latter process can follow three different evolutionary models depending on the material behaviour as follows.

(IVa) Differential subsidence of mid-cohesive material, giving rise to gentle passive bending that accommodates length variation without inducing any 'space problem' (*sagging*, according to the classification proposed by Gutiérrez, Guerrero & Lucha, 2008). Normal faults could also appear where bending involves extra layer-parallel stretching.

(IVb) Sudden collapse of subsoil cavities in a highly cohesive rigid cover, progressing from vault-shaped tensile cracks.

(IVc) Non-differential subsidence of moderately cohesive material that shows low external cohesion with respect to the bounding stable material. Shortening from the original length L_0 to the new length L_1 is accommodated by contractional structures (reverse faults or reverse kink-bands). These are mainly concentrated near the boundaries, although they can propagate inwards depending on the ability of the sinking body to transfer stress.

6. Geophysical study

Taking into account that the quarry walls essentially provide 2D observations, a geophysical survey has been carried out in order to investigate the 3D geometry of some structures.

Concerning the magnetic survey, the susceptibility values range from 0.05×10^{-4} to 0.8×10^{-4} SI for marl, and from 0.1×10^{-5} to 0.7×10^{-5} SI for sand and gravel. *A priori*, these values show enough contrast to define the main observed structures (collapses mainly filled with sand and some gravel, and diapirs constituted by Miocene gypsum and marl). The objective was to establish or discard the continuity of deformation structures in areas where they do not crop out. However, the results (after correction for the magnetic drift) were uniform, with variations of less than 10 nT. Gradient values are also uniform and range from 2.2 to -2 nT m^{-1} (Fig. 13a). Moderate differences are found between the quarry floor (low values at the central-eastern sector) and the natural landscape (medium values at the northern, western and southern surrounding sectors) due to the absence/presence of natural soil. The highest values along the borders of the surveyed area are due to the presence of agricultural soils or quarry stocks. In any case, the sharp localized anomalies detected at the southwestern sector of the quarry (D in Fig. 13a) coincide with a small diapiric structure cropping out on the quarry walls (D in Fig. 3a), confirming that this structure has no lateral continuity.

The electromagnetic (EM) survey reveals the existence of a low conductivity strip at both high and low frequencies (Fig. 13b, c), which reflects the behaviour
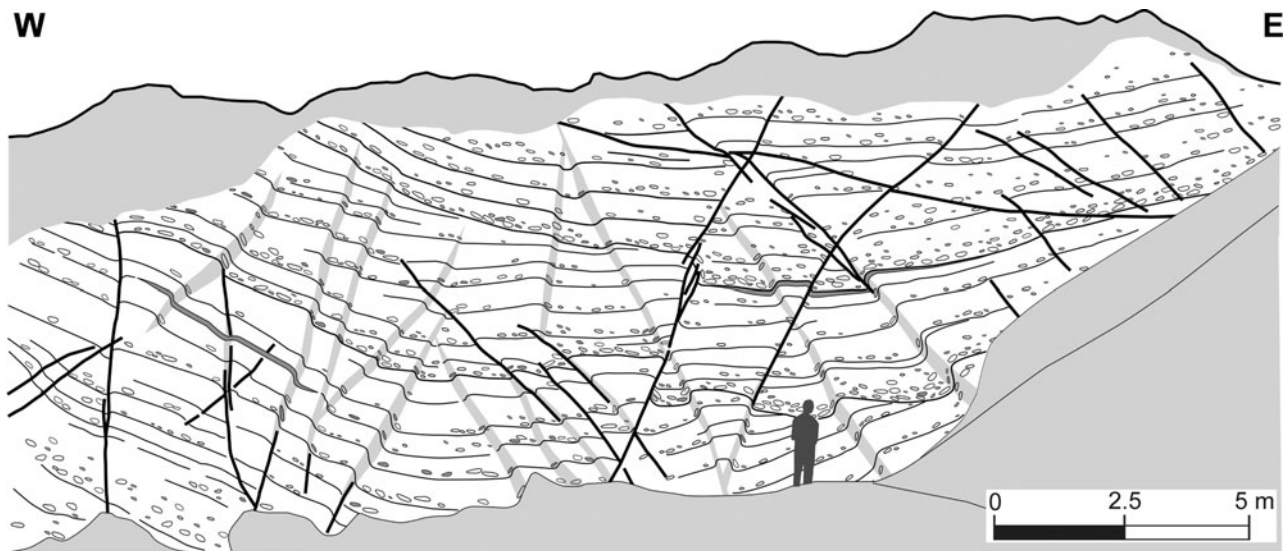
Figure 11. High-angle reverse faults and kink bands deforming gravel and sand beds close to the diapir cropping out in sector 2 (see Fig. 9).
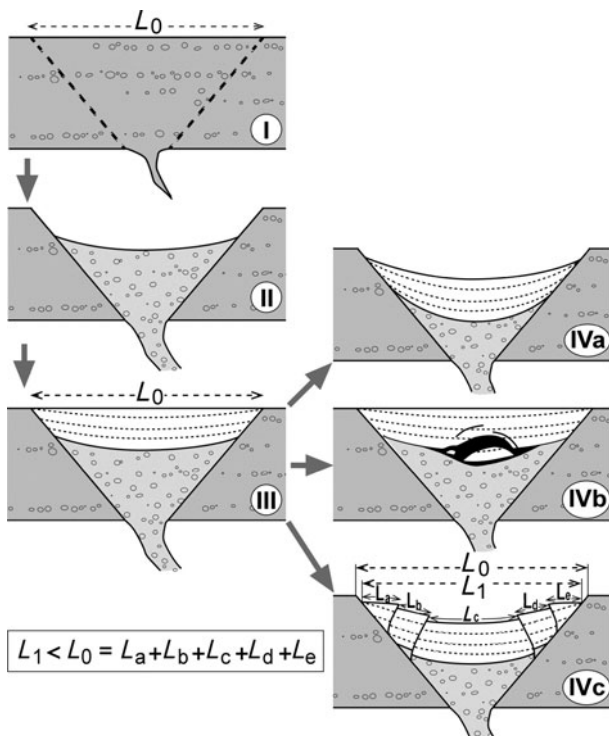

Figure 12. Kinematical model that explains horizontal shortening in karst subsidence structures. See detailed explanation in text.

of shallow and deep materials, respectively. The curved morphology of this strip and its position, coincident with the synform located close to the eastern diapir, suggest that it could represent a segment of the rim syncline (RS in Fig. 13b, c) associated with this diapir, which was therefore active during sedimentation. The large thickness of Quaternary materials is the reason for the low conductivity of this zone.

Ground-penetrating radar (GPR) profiles acquired from the quarry floor allow us to infer variations in

depth of the Miocene bedrock and the presence of conjugate faults. In addition, the GPR profiles acquired to characterize the main collapse structure gave excellent results. The profile made with the 100 MHz antenna on a berm located over this structure produced a high-resolution image (Fig. 13d) in which the U-shaped fill shown in Figure 6a is easily recognizable. Comparing this profile with other profiles acquired from the quarry floor close to the toe of the same wall, the lateral continuity of this U-shaped geometry could not be evidenced; this supports the interpretation of this structure as a karst collapse.

The diapirs of the western sector were also surveyed; however, not enough accurate results were obtained. The reasons for this are probably the irregular topography of the zone where the profile was made and the diffuse contact between Pleistocene and Miocene materials (with numerous enclaves of plastically deformed gravels included in marls).

7. Discussion

After describing and analysing the distinct deformation structures in the studied quarry, two main issues merit discussion and synthesis in order to determine the consequences of synsedimentary deformation in terrigenous sediments: (i) diagnostic criteria that can be used for distinguishing genetic types and their kinematical models; and (ii) interaction mechanisms between different deformation and deposition processes.

7.a. Diagnostic criteria for distinguishing genetic deformation types

Diagnostic criteria should initially be based on geometrical and kinematical analysis of deformation structures. First, 3D geometric features at the surface and the subsoil (the latter supported by results of geophysical
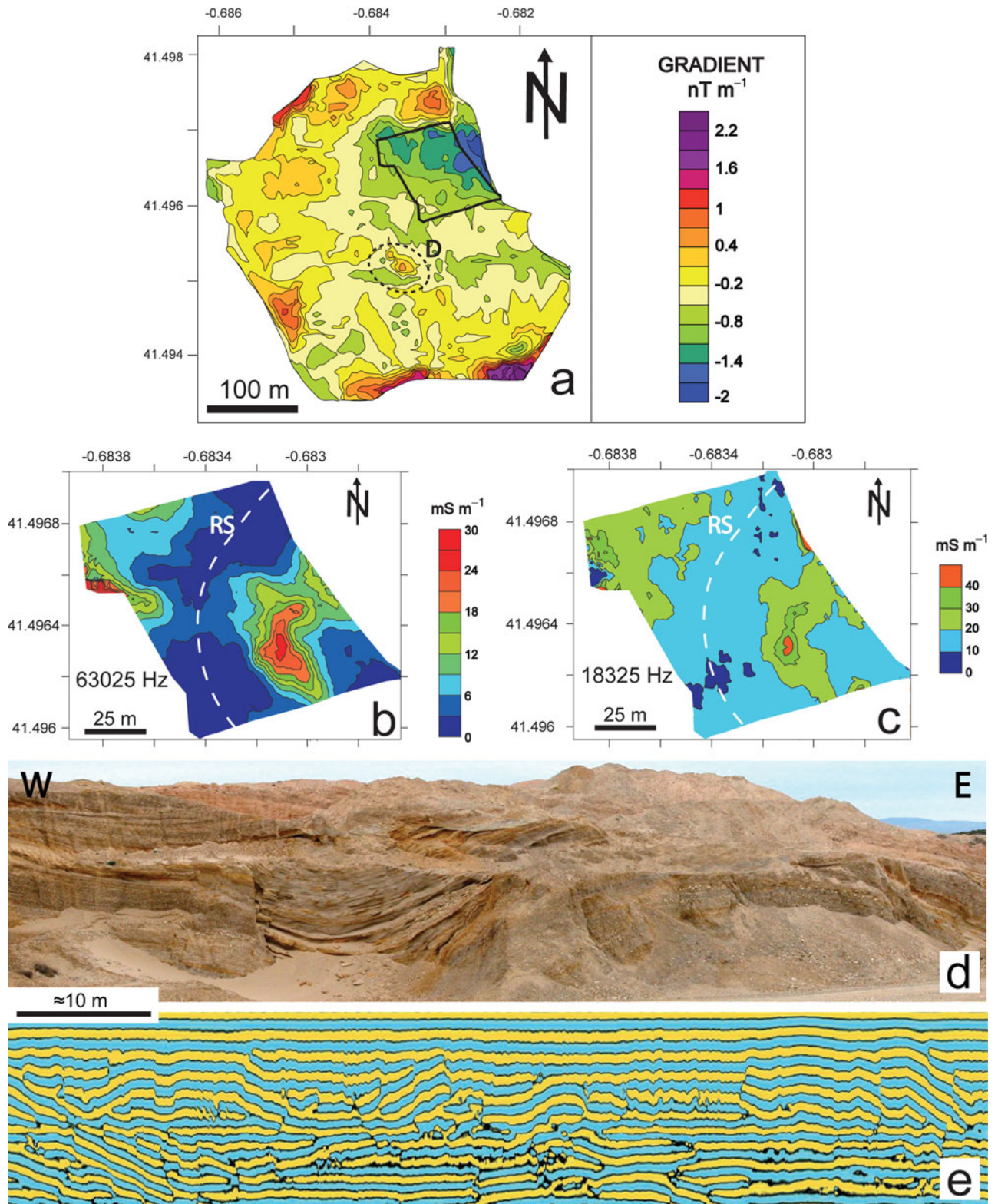
Figure 13. (Colour online) Most representative results of the geophysical survey (see location of the studied areas in Fig. 1c). (a) Geomagnetic survey (gradient map) of the quarry and its neighbouring area; D: diapir. (b, c) Electromagnetic survey of a selected zone of the quarry floor depicted in (a); apparent conductivity anomalies at high (63,025 Hz) and low (18,325 Hz) frequencies, respectively; RS: rim syncline. (d) GPR section along the berm of the northern quarry wall (sectors 4 and 5 in Fig. 9). (e) Panoramic field view of the above mentioned sector, to be compared with the GPR section.

survey) can constrain our genetic hypotheses: planar rupture boundaries and elongated geophysical anomalies will generally be attributed to tectonic faults, whereas nearly rounded, either positive or negative

structures, will be interpreted as diapirs or karst collapses, respectively. Constraints are less narrow when only 2D exposures are available; in such situations, the kinematical approach becomes critical. In most cases,

kinematical analysis will easily provide a consistent interpretation of the relative motions at the boundaries of such structures, both in the vertical (upwards v. downwards moving domains) and the horizontal axes (contractional v. extensional deformation). Nevertheless, such attributes are not exclusive to each genetic type so the kinematical analysis of structures does not properly discern their origin.

Considering the relative vertical movements, their kinematical patterns do not allow tectonic faults from diapirs or karst collapses to be distinguished in the absence of complete 3D geometric reconstructions. Moreover, distinguishing diapirs from palaeodolines can be difficult (except in the case of isolated rock bodies that have clearly risen or sunk with respect to a predeformational, recognizable marker).

Evidence of widespread horizontal extension accommodated by normal faults should generally be attributed to regional tectonics, once the dynamical consistency of the dominant fault systems with the regional stress field has been tested. In our case, such consistency is perfectly accomplished for normal faults striking close to NNW–SSE (approximate regional trend of S_{Hmax}). Nevertheless, the transition to NNE–SSW-trending σ_2 trajectories, as well as local switching to orthogonal ENE–WSW- or ESE–WNW-trending trajectories, is also common (Simón, 1989; Cortés *et al.* 1996; Simón *et al.* 1999; Simón, Arlegui & Liesa, 2008). In contrast, stretching occurring on diapir crests and doline boundaries is a local process clearly controlled by the rising or the sinking domain, so does not give rise to penetrative and systematic faults and fractures. In any case, the possibility of identifying such local fault patterns depends on the availability of an adequate map view of structures.

Horizontal contraction could be caused by regional compressional tectonics, but the tectonic extensional setting of the Ebro Basin during Quaternary time leads us to rule out such a hypothesis. Local contractional structures could also be induced by piercing diapirs and, under some conditions, by karst collapses. Concerning the horizontal length balance, there is an essential difference between a tectonic normal fault and a local vertical displacement produced by diapiric intrusion or karst collapse: a normal fault accommodates horizontal extension externally imposed by the geodynamic framework, while a diapir or a collapse evolves without intrinsic far-field shortening or stretching. The possibility that either contractional or extensional structures were associated with diapirs or karst collapses therefore depends exclusively on their own kinematical mechanisms.

Both diapirism and karst subsidence essentially consist of vertical migration of material that occupies a volume formerly occupied by another material. In both types of structures, vertical displacement of rock bodies showing heterogeneous rheology frequently induces 'space problems', that is, a misfit of displacement trajectories that results in local, usually radial shortening or stretching. Nevertheless, the difference between the

processes remain: (i) in karst subsidence, material sinks to occupy a void left by previously dissolved or dragged rocks, therefore space problems should not necessarily occur; or (ii) the core of a diapir intrudes into a rock body where no previous space is available, producing a wedge effect that tends to move the host rock away; contractional deformation is therefore intrinsic to the process. This notion was emphasized by Simón & Soriano (1986) and Soriano & Simón (1995), who suggested that actual reverse rupture surfaces are characteristic of diapirs whereas 'pseudo-reverse' contacts associated with collapse structures are in fact vault-shaped tensile cracks produced by the sudden falling of rigid blocks into an open void. Nevertheless, our detailed study of the complex U-shaped structure described in Section 4.b demonstrates that true contractional structures can also develop at the margins of a doline under the conditions stated in Section 5.b and Figure 12.

In summary, structural analysis shows that both extensional and contractional structures can be associated with each of the three analysed deformation processes. Extensional contacts may represent either tectonic faults, fractures developed at diapir crests or funnel-shaped sinkhole boundaries. Contractional contacts might arise from compressional tectonic stress fields (which is not the case in the Ebro Basin), but also from lateral compression induced by wedge action of piercing diapirs or karst subsidence of a sedimentary body with high internal cohesion but low external cohesion with respect to the bounding rock.

7.b. Interaction between different deformation and deposition processes

Further difficulty for the genetic diagnosis of deformational structures arises as different genetic processes (tectonic fracturing, karst subsidence, diapiric intrusion) frequently interact. Our detailed analysis allows us to approach the mechanisms whereby one of them triggers or influences the other. Further, the sedimentological study demonstrates that coeval deformation modifies the sedimentary environment configuration, especially in controlling the accommodation space.

An example of interaction between tectonic faulting, karst subsidence and sedimentary processes is represented by the conspicuous U-shaped structure. Although the final structure has been characterized as a palaeodoline, it is bounded by tectonic faults that could produce a fraction of the total subsidence and controlled the location of the karst sink centre (by creating discontinuities that favoured water infiltration and modifying the mechanical properties of the Quaternary cover). The resulting hole provided physical space for fluvial and aeolian sediments to be accumulated and preserved from subsequent fluvial erosion, as occurs in similar cases described by Luzón *et al*. (2008, 2012).

From the observations made, the complete evolution of this complex structure can be reconstructed; it essentially involves earlier synsedimentary movement on the eastern limb, then on the western limb. Westwards

expansion of the central sand body, then cut by the western fault, constitutes the critical evidence for such a deformation sequence. The evolutionary stages can be described in detail (Fig. 14) as follows.

1. During Early Pleistocene clastic sedimentation in a fluvial braided environment occured above Miocene evaporites. Both stratigraphical units were cut by a fault zone that triggered karst dissolution at depth.

2. Faulting and dissolution caused subsidence at the eastern boundary of the structure. Continuous sinking generated thickening of gravel bodies that produced a growth strata structure. Subsequent bending induced fracture propagation upwards.

3. The created hole acted as a sedimentary trap, in which small sand dunes accumulated constructing a sand body that expanded westwards. Episodically, subsidence induced relative rising of the water table, favouring lutite adhesion onto a damp surface. In a context dominated by high-energy and laterally migrating channels, such local subsidence prevented the fine-grained sediments from be eroded. Soft-sediment deformation structures in the lutite levels (Fig. 6g) were probably related to sudden sinking episodes.

4. Movement at the eastern limb vanished while the uppermost sands were deposited. Most deformation was transferred to the western limb, where a tectonic N–S-trending fault appeared, then favoured renewed karstic subsidence. The depocentre, then filled with palustrine lutites, moved to the west with respect to the previous stage.

5. Subsidence finished and new braided fluvial gravels were deposited over the whole deformed zone.

In the described evolutionary model the accommodation space and the accumulation of aeolian sands coincide, as well as at other sites formerly studied in the Ebro Basin (Luzón *et al.* 2012; Gil *et al.* 2013*a*). However, this is not common (Kocurek & Havholm, 1993; Tirsgaard & Øxnevad, 1998). Aeolian sand is only preserved from erosion during subsequent flooding episodes if it is deposited below the baseline of erosion, which is determined by subsidence and the groundwater table (Clemmensen & Dam, 1973; Fryberger & Schenk, 1988; Kocurek & Havholm, 1993; Sweet, 1999; Mountney & Russell, 2009). In a tectonically stable setting a rising or falling groundwater table will have an impact on aeolian sediment preservation (Clemmensen & Dam, 1973). In contrast, base level fluctuations are not only climatically driven in some scenarios; active subsidence can play an important role in aeolian preservation (Rodríguez-López *et al.* 2008). In the study case, and taking into account that large aeolian dune foresets have been preserved, a relatively rapid subsidence should be invoked which could not be accomplished just by sediment compaction. Preservation of aeolian deposits was clearly favoured by karst and tectonic subsidence, which in turn generated the necessary increase in accommodation space.

Diapirism also seems to have been partially controlled by tectonic faulting. Where vertical displacements produced by tectonic faults trigger diapirs, these
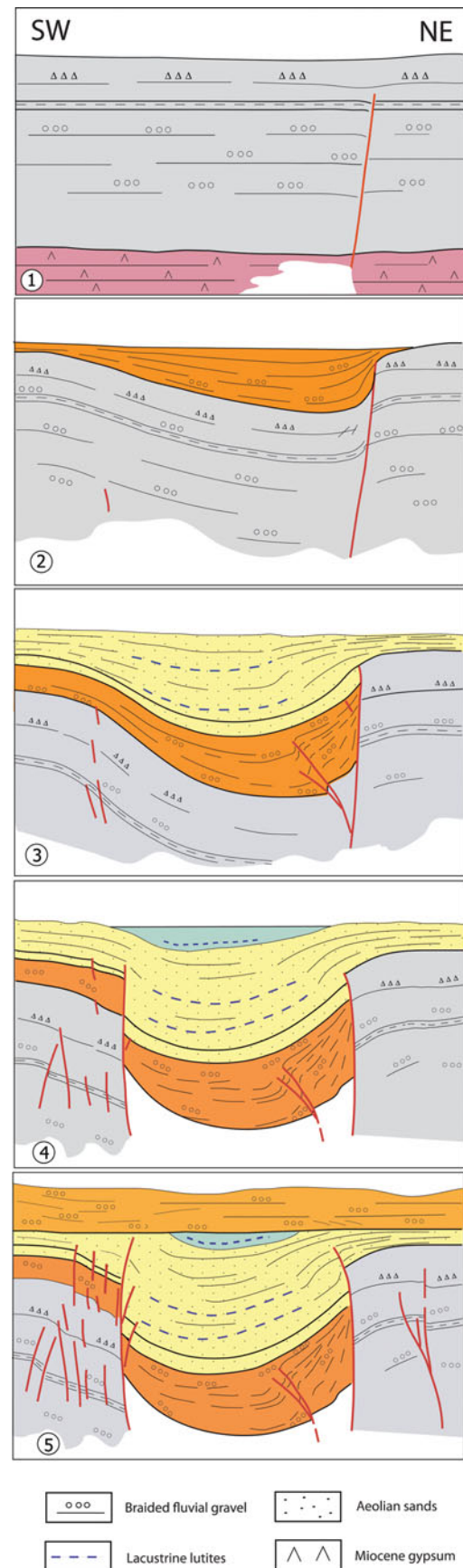

Figure 14. (Colour online) Evolutionary model of the U-shaped structure cropping out in sectors 4–5, representative of the interaction between tectonic faulting, karst subsidence and sedimentation in Pleistocene deposits of the central Ebro basin. See detailed explanation in the text.

are expected to show overall elongation and planar intrusive boundaries parallel to faults. This setting has been recognized in: (i) the elongated geometry of the eastern diapir (sectors 1 and 2), whose western limb crops out as a NNW–SSE-trending monocline along the quarry front; and (ii) the predominance of rupture surfaces, high-angle reverse faults and kink-bands showing the same N–S- to NNW–SSE-strike as normal faults. Such control could be substantiated by differences of lithostatic load induced by normal faults, which triggered migration of plastic Miocene materials (e.g. Pflug, 1973; Simón & Soriano, 1986; Vendeville & Jackson, 1992; Jackson, Vendeville & Schultz-Ela, 1994).

No evidence about the interaction between diapiric and karst processes has been found in the studied area. The mechanism proposed by Benito & Casas (1987) to explain the occurrence of diapirs in terrace fluvial deposits thickened by karst subsidence (gravitational instability due to rapid loading and excess of fluid pressure) seems not to have operated in the studied case, since the thickness of the sedimentary cover overlying diapirs is low. In addition, the presence of uplifted, intruding evaporite bodies should not be invoked as a control for karst dissolution: this is a widespread phenomenon in the central Ebro Basin because the occurrence of evaporites at the shallow subsoil is pervasive throughout the region.

8. Conclusions

Genetic diagnosis of varied types of deformation structures in Pleistocene deposits of the central Ebro Basin has been achieved by combining structural and sedimentological analysis, as well as geophysical exploration of shallow subsoil levels.

Brittle structures of tectonic origin (essentially normal faults) are distinguished by their planar and elongated attitude as well as their preferred orientations, either determined by the remote stress field (N–S- to NNW–SSE-striking faults and fractures, roughly parallel to the regional trend of $S_{Hmax} = \sigma_2$ trajectories) or modified by inherited faults (occasional E–W- to ENE–WSW-striking fractures due to local switching σ_2 and σ_2 stress axes).

In contrast, karst collapses and diapirs are local, broadly cylindrical structures, whose 3D geometry has been characterized by means of geophysical techniques. Diapirs and palaeodolines have been discriminated from each other where isolated rock bodies have clearly risen or sunk with respect to a predeformational recognizable marker. Where such a reference level is not available, vertical differential movements have been interpreted from kinematical analysis of internal deformation; 'positive' and 'negative' structures are not discernible, however.

Tectonic faults accommodate horizontal mainly E–W- to ENE–WSW-oriented stretching consistent with the regional extensional deformation regime. The occurrence of contractional structures does not fit such a tectonic framework. Nevertheless, these can be locally generated by: (i) lateral compression induced by wedge action of piercing diapirs; and (ii) karst subsidence of a sedimentary body with high internal cohesion and low external cohesion with respect to the bounding rock.

Interaction between different deformation and sedimentary processes did occur at the central Ebro Basin during Early Pleistocene times. Mass loss inducing local subsidence was triggered by tectonic faults (the latter acting as preferred paths for water flow, and hence dissolution or piping). Diapirism has been partially controlled by tectonic faulting, giving rise to elongated diapirs bounded by planar intrusive surfaces roughly parallel to faults.

All these deformation processes occurred while continental (fluvial, aeolian and lacustrine) sedimentation was in progress. Deformation closely controlled the accommodation space. Holes created by tectonic and karstic subsidence acted as sedimentary traps in which, in addition, the groundwater table fell. Both factors allowed sand dunes and episodic palustrine lutites to be accumulated and then preserved.

References

ANADÓN, P., CABRERA, L., COLOMBO, F., MARZO, M. & RIBA, O. 1986. Syntectonic intraformational unconformities in alluvial fan deposits, eastern Ebro basin margins (NE Spain). In *Foreland Basins* (eds P. Allen & P. Homewood), pp. 259–71. IAS, Special Publication no. 8.

ANDEWEG, B., DE VICENTE, G., CLOETHING, S., GINER, J. & MUÑOZ-MARTÍN, A. 1999. Local stress fields and intraplate deformation of Iberia: variations in spatial and temporal interplay of regional stress sources. *Tectonophysics* **305**, 153–64.

ARLEGUI, L. E. & SIMÓN, J. L. 2000. Fracturación y campos de esfuerzos en el Cuaternario del sector central de la Cuenca del Ebro (NE España). *Cuaternario y Geomorfología* **14**, 11–20.

ARLEGUI, L. E. & SIMÓN, J. L. 2001. Geometry and distribution of regional joint sets in a non-homogeneous stress field: case study in the Ebro basin (Spain). *Journal of Structural Geology* **23**, 297–313.

ARLEGUI, L. E. & SORIANO, M. A. 2003. An example of a comparison between Thematic Mapper and radar images in the central Ebro basin. *International Journal of Remote Sensing* **24**, 457–74.

ASCHOFF, J. L. & SCHMITT, J. G. 2008. Enhancing growth strata analysis by distinguishing syntectonic unconformity types. *Journal of Sedimentary Research* **78**, 608–23.

BANHAM, S. G., MOUNTNEY, N. P., KANE, I. & MCCAFFERY, W. D. 2011. Controls on sedimentary evolution and preservation of dryland fluvial systems inactively subsiding

salt-walled mini-basins (Salt Anticline Region, Utah). In *28th IAS Meeting of Sedimentology, Abstracts* (eds B. Bádenas, M. Aurell and A. M. Alonso-Zarza), pp. 72. Zaragoza, Spain.

BECK, B. F. 2004. Soil piping and sinkhole failures. In *Encyclopedia of Caves* (ed. W. B. White), pp. 523–8. New York: Elsevier.

BENITO, G. & CASAS, A. M. 1987. Small-scale deformations in Quaternary deposits in the northeastern Iberian peninsula. *Géologie Méditerranéenne* **14**, 233–43.

BENITO, G., PÉREZ-GONZÁLEZ, A., GUTIÉRREZ, F. & MACHADO, M.J. 1998. River response to Quaternary subsidence due to evaporite solution (Gállego River, Ebro Basin, Spain). *Geomorphology* **22**, 243–63.

BENITO, G., PÉREZ-GONZÁLEZ, A. & MACHADO, M. J. 2000. Geomorphological and sedimentological features in Quaternary fluvial systems affected by solution-induced subsidence (Ebro Basin, NE-Spain). *Geomorphology* **33**, 209–24.

BLISSENBACH, E. 1954. Geology of alluvial fans in semiarid regions. *Geological Society of America Bulletin* **65**, 175–90.

BRIANT, R., BATEMAN, M. D., COOPE, G. R. & GIBBARD, P. L. 2005. Climatic control on Quaternary fluvial sedimentology of a Fenland Basin river, England. *Sedimentology* **52**, 1397–423.

BULL, W. B. 1968. Alluvial fans. *Journal of Geological Education* **16**, 101–6.

CALAFORRA, J. M. & PULIDO-BOSCH, A. 1999. Gypsum karst features as evidence of diapiric processes in the Betic Cordillera, Southern Spain. *Geomorphology* **29**, 251–64.

CLEMMENSEN, L. B. & DAM, G. 1973. Aeolian sand-sheet deposits in the Lower Cambrian Neksø Sandstone Formation, Bornholm, Denmark: sedimentary architecture and genesis. *Sedimentary Geology* **83**, 71–85.

COLOMER, M. V., NAVARRO, J. J., HERNÁNDEZ, A. & RAMÍREZ, J. I. 2006. Mapa geológico de España: Pina de Ebro (412): Instituto Geológico y Minero de España, scale 1:50000, 1 sheet.

CORTÉS, A. L., LIESA, C. L., SIMÓN, J. L., CASAS, A. M., MAESTRO, A. & ARLEGUI, L. E. 1996. El campo de esfuerzos compresivo neógeno en el NE de la Península Ibérica. *Geogaceta* **20**, 806–9.

DAVIES, N. S., TURNER, P. & SANSOM, I. J. 2004. Soft-sediment deformation structures in the Late Silurian Stubdal Formation: the result of seismic triggering. *Norwegian Journal of Geology* **85**, 233–43.

DOGAN, U. 2005. Land subsidence and caprock dolines caused by subsurface gypsum dissolution and the effect of subsidence on the fluvial system in the Upper Tigris Basin (between Bismil-Batman, Turkey). *Geomorphology* **71**, 389–401.

FOLK, R. L. 1966. A review of grain size parameters. *Sedimentology* **6**, 73–93.

FORD, D. C. 1997. Principal features of evaporite karst in Canada. *Carbonates and Evaporites* **12**, 15–23.

FORD, D. & WILLIAMS, P. 1989. *Karst Geomorphology and Hydrology*. London: Capman & Hall.

FRYBERGER, S. G. & SCHENK, C. J. 1988. Pin stripe lamination: a distinctive feature of modern and ancient eolian sediments. *Sedimentary Geology* **55**, 1–15.

GARCÍA-CASTELLANOS, D., VERGÉS, J., GASPER-ESCRIBANO, J. & CLOETINGH, S. 2003. Interplay between tectonics, climate and fluvial transport during the Cenozoic evolution of the Ebro Basin (NE Iberia). *Journal of Geophysical Research* **108**, 1–18.

GIL, H., LUZÓN, A., SORIANO, M. A., CASADO, I., PÉREZ, A., YUSTE, A., PUEYO, E. & POCOVÍ, A. 2013*a*. Stratigraphic architecture of alluvial-aeolian systems developed on active karst terrains: an Early Pleistocene example from the Ebro Basin. *Sedimentary Geology* **296**, 122–41.

GIL, H., PUEYO, E., PALMA-RODRIGUES, A., SORIANO, M. A., LUZÓN, A., POCOVÍ, A., PÉREZ, A. & YUSTE, A. 2013*b*. Caracterización paleomágnetica y anisotropía de susceptibilidad magnética (ASM) de las terrazas antiguas del río Ebro. *Geogaceta* **53**, 129–32.

GRUSZKA, B. & LOON, A. J. 2007. Pleistocene glaciolacustrine breccias of seismic origin in an active graben (central Poland). *Sedimentary Geology* **193**, 93–104.

GUERRERO, J., GUTIÉRREZ, F. & LUCHA, P. 2004. Paleosubsidence and active subsidence due to evaporite dissolution in the Zaragoza area (Huerva River valley, NE Spain): processes, spatial distribution and protection measures for transport routes. *Engineering Geology* **72**, 309–29.

GUGLIELMO, G., JACKSON, M. P. A. & VENDEVILLE, B. C. 1997. Three-dimensional visualization of salt walls and associated fault systems. *AAPG Bulletin* **81**, 46–61.

GUSTAVSON, T. C. 1986. Geomorphic development of the Canadian River Valley, Texas Panhandle: an example of regional salt dissolution and subsidence. *Geological Society of America Bulletin* **97**, 459–72.

GUTIÉRREZ, F., GUERRERO, J. & LUCHA, P. 2008. A genetic classification of sinkholes illustrated from evaporite paleokarst exposures in Spain. *Environmental Geology* **53**, 993–1006.

HEIN, F. J. & WALKER, R. G. 1977. Bar evolution and development of stratification in the gravelly, braided Kicking Horse river, British Columbia. *Canadian Journal of Earth Sciences* **14**, 562–70.

HEMPTON, M. R. & DEWEY, J. F. 1983. Earthquake-induced deformational structures in young lacustrine sediments, East Anatolian fault, south-east Turkey. *Tectonophysics* **98**, T7–T14.

HERRAIZ, M., DE VICENTE, G., LINDO-ÑAUPARI, R., GINER, J., SIMÓN, J. L., GONZÁLEZ-CASADO, J. M., VADILLO, O., RODRÍGUEZ-PASCUA, M. A., CICUÉNDEZ, J. I., CASAS, A., CABAÑAS, L., RINCÓN, P., CORTÉS, A. L., RAMÍREZ, M. & LUCINI, M. 2000. The recent (upper Miocene to Quaternary) and present tectonic stress distributions in the Iberian Peninsula. *Tectonics* **19**, 762–86.

HUNTER, R. E. 1977. Basic types of stratification in small eolian dunes. *Sedimentology* **24**, 361–87.

HUNTER, R. E. 1981. Stratification styles in eolian sandstones: some Pennsylvanian to Jurassic examples from the western interior U.S.A. In *Recent and Ancient Nonmarine Depositional Environments* (eds F. G. Ethridge & R. M. Flores), pp. 315–329. SEPM, Special Publication no. **31**.

JACKSON, M. P. A., VENDEVILLE, B. C. & SCHULTZ-ELA, D. D. 1994. Structural dynamics of fault systems. *Annual Review of Earth and Planetary Sciences* **22**, 93–117.

KOCUREK, G. 1991. Interpretation of ancient eolian sand dunes. *Annual Review of Earth and Planetary Sciences* **19**, 43–75.

KOCUREK, G. & DOTT, R. 1981. Distinctions and uses of stratification types in the interpretation of eolian sand. *Journal of Sedimentary Petrology* **51**, 579–95.

KOCUREK, G. & HAVHOLM, K. G. 1993. Eolian sequence stratigraphy - a conceptual framework. In *Siliciclastic Sequence Stratigraphy, Recent Developments and Applications* (eds P. Weimer & H. W. Posamentier),

pp 393–409. American Association of Petroleum Geologists, Memoir no. **58**.

LANCASTER, N. 1981. Grain size characteristics of Namib Desert linear dunes. *Sedimentology* **28**, 115–22.

LANCASTER, N. 1986. Grain-size characteristics of linear dunes in the southwestern Kalahari. *Journal of Sedimentary Petrology* **56**, 395–400.

LIESA, C. L. & SIMÓN, J. L. 2009. Evolution of intraplate stress fields under multiple compressions: the case of the Iberian Chain (NE Spain). *Tectonophysics* **474**, 144–59.

LOOFF, K. M. & LOOFF, K. M. 2000. Subsidence, sinkholes, and piping associated with Gulf Coast salt domes. *Proceedings SMRI Fall 2000 Meeting*, San Antonio, Texas, pp. 275–301.

LUZÓN, A., PÉREZ,, A., POCOVÍ, A., SORIANO, M. A., GIL, H., RODRÍGUEZ-LÓPEZ, J. P. & SIMÓN, J. L. 2011. Sedimentary record related to the evolution of Quaternary dolines in the central Ebro Basin (Spain). *Geo-Guias* **7**, 199–226.

LUZÓN, A., PÉREZ, A., SORIANO, M. A. & POCOVÍ, A. 2008. Sedimentary record of Pleistocene paleodoline evolution in the Ebro basin (NE Spain). *Sedimentary Geology* **205**, 1–13.

LUZÓN, A., RODRÍGUEZ-LÓPEZ, J. P., PÉREZ,, A., SORIANO, M. A., GIL, H. & POCOVÍ, A. 2012. Karst subsidence as a control on the accumulation and preservation of aeolian deposits: a Pleistocene example from a proglacial outwash setting, Ebro Basin, Spain. *Sedimentology* **59**, 2199–225.

MARQUÉS, L. A., SANTOS, J. A., ESNAOLA, J. M. & GIL MARÍN, C. 1998. Mapa geológico de España: Fuentes de Ebro (384): Instituto Geológico y Minero de España, scale 1:50000, 2nd series, 1 sheet.

MASTALERZ, K. & WOJEWODA, J. 1993. Alluvial-fan sedimentation along an active strike-slip fault: plio- Pleistocene Pre-Kaczawa fan, SW Poland. In *Alluvial Sedimentation* (eds M. Marzo & C. Puigdefábregas), pp. 293–304. IAS, Special Publication no. **17**.

MIALL, A. D. 1978. Lithofacies types and vertical profile models in braided river deposits: a summary. In *Fluvial Sedimentology* (ed. A. D. Miall), pp. 597–604. Canadian Society of Petroleum Geology, Memoir no. **5**.

MIALL, A. D. 1996. *The Geology of Fluvial Deposits. Sedimentary Facies, Basin Analysis, and Petroleum Geology*. Berlin: Springer-Verlag.

MORGAN, J. P., COLEMAN, J. M. & GAGLIANO, S. M. 1968. Mudlumps: diapiric structures in the Mississippi delta sediments. In *Diapirim and Diapirs* (eds J. Braunstein & G. D. O'Brien), pp. 145–61. American Association of Petroleum Geology, Memoir no. **8**.

MOUNTNEY, N. P. 2006*a*. Eolian facies models. In *Facies Models Revisited* (eds R. G. Walker & H. Posamentier), pp. 19–83. SEPM, Memoir no. **84**.

MOUNTNEY, N. P. 2006*b*. Periodic accumulation and destruction of aeolian erg sequences in the Permian Cedar Mesa Sandstone, White Canyon, southern Utah, USA. *Sedimentology* **53**, 789–823.

MOUNTNEY, N., HOWELL, J., FLINT, S. & JERRAM, D. 1999. Relating aeolian bounding-surface geometries to the bed forms that generated them: Etjo Formation, Cretaceous, Namibia. *Geology* **27**,159–62.

MOUNTNEY, N. P. & RUSSELL, A. J. 2009. Aeolian dune-field development in a water table-controlled system: Skeiðarársandur, Southern Iceland. *Sedimentology* **56**, 2107–31.

MUÑOZ, A., ARENAS, C., GONZÁLEZ, A., LUZÓN, A., PARDO, G., PÉREZ, A. & VILLENA, J. 2002. Ebro Basin (north-eastern Spain). In *The Geology of Spain* (eds W. Gibbons & T. Moreno), pp. 370–85. London: Geological Society.

MUÑOZ, A. & CASAS, A. M. 1997. The Rioja Trough (N Spain): tectosedimentary evolution of a symmetric foreland basin. *Basin Research* **9**, 65–85.

NEMEC, W. & STEEL, R. J. 1988. *Fan Deltas: Sedimentology and Tectonic Setting*. Glasgow: Blakie.

PARDO, G., ARENAS, C., GONZÁLEZ, A., LUZÓN, A., MUÑOZ, A., PÉREZ, A., PÉREZ RIVARÉS, F. J., VÁZQUEZ-URBEZ, M. & VILLENA, J. 2004. La Cuenca del Ebro. In *Geología de España* (ed. J. A. Vera), pp. 533–43. Madrid: IGME & Sociedad Geológica de España.

PFLUG, R. 1973. El diapiro de Estella. *Munibe-Sociedad de Ciencias Naturales Aranzadi* **25**, 171–202.

PUEYO-ANCHUELA, O., CASAS-SAINZ, A. M., SORIANO, M. A., POCOVÍ-JUAN, A., IPAS-LLORÉNS, J. F. & ANSÓN-LÓPEZ, D. 2010. Integrated geophysical and building damages study of karst effects in the urban area of Alcalá de Ebro, Spain. *Zeitschrift für Geomorphologie* **54**, 221–36.

PURDY, E. G. 1974. Karst-determined facies patterns in British Honduras: Holocene carbonate sedimentation model. *AAPG Bulletin* **58**, 825–55.

QUIRANTES, J. 1978. *Estudio Sedimentológico y Estratigráfico del Terciario Continental de los Monegros*. Ph.D. thesis, Instituto Fernando el Católico (CSIC), Diputación Provincial de Zaragoza. Published thesis.

RIBA, O. 1976. Syntectonic unconformities of the Alto Cardener, Spanish Pyrenees: a genetic interpretatio. *Sedimentary Geology* **15**, 213–33.

RIBA, O., REGUANT, S. & VILLENA, J. 1983. Ensayo de síntesis estratigráfica y evolutiva de la Cuenca terciaria del Ebro. In *Libro Jubilar J.M. Ríos, Geología de España (II)* (ed. J. M. Comba), pp. 131–59. Madrid: Instituto Geológico y Minero de España.

RODRÍGUEZ-LÓPEZ, J. P., DE BOER, P. L., MELÉNDEZ, N., SORIA, A. R. & PARDO, G. 2006. Windblown desert sands in coeval shallow marine deposits a key for the recognition of coastal ergs; mid-Cretaceous Iberian Basin, Spain. *Terra Nova* **18**, 314–20.

RODRÍGUEZ-LÓPEZ, J. P., MELÉNDEZ, N., DE BOER, P. L. & SORIA, A. R. 2008. Aeolian sand sea development along the Mid-Cretaceous Western Tethyan Margin (Spain): erg sedimentology and palaeoclimate implications. *Sedimentology* **55**, 1253–92.

RUST, B. R. 1978. A classification of alluvial channel systems. In *Fluvial Sedimentology* (ed. A. D. Miall), pp. 187–98. Canadian Society of Petroleum Geology, Memoir no. **5**.

SCHERER, C. M. S. 2000. Eolian dunes of the Botucatu Formation (Cretaceous) in southernmost Brazil: morphology and origin. *Sedimentary Geology* **137**, 63–84.

SEILACHER, A. 1969. Fault graded beds interpreted as seismites. *Sedimentology* **13**, 155–59.

SEILACHER, A. 1984. Sedimentary structures tentatively attributed to seismic events. *Marine Geology* **55**, 1–2.

SHUKLA, U. K. 2009. Sedimentation model of gravel-dominated alluvial piedmont fan, Ganga Plain, India. *International Journal of Earth Sciences* **98**, 443–59.

SILVA, P. G., LÓPEZ RECIO, M., GONZÁLEZ HERNÁNDEZ, F. M., TAPIAS, F., ALARCÓN, A., CUARTERO, F., EXPÓSITO, A., LÁZARO, A., MANZANO, I., MARÍN, D., MORÍN, J. & YRAVEDRA, J. 2008. Datos geoarqueológicos de la terraza compleja del Manzanares entre el sector del 12 de Octubre y la desembocadura del arroyo Butarque (Villaverde, Madrid). *Cuaternario y Geomorfología* **22**, 47–70.

SIMÓN, J. L. 1989. Late Cenozoic stress field and fracturing in the Iberian Chain and Ebro Basin (Spain). *Journal of Structural Geology* **11**, 285–94.

SIMÓN, J. L. 2006. El registro de la compresión intraplaca en los conglomerados de la cuenca terciaria de Aliaga (Teruel, Cordillera Ibérica). *Revista de la Sociedad Geológica de España* **19**, 163–79.

SIMÓN, J. L., ARLEGUI, L. E. & LIESA, C. L. 2008. Stress partitioning: a practical concept for analysing boundary conditions of brittle deformation. *Geodinamica Acta* **53**, 1057–65.

SIMÓN, J. L., ARLEGUI, L. E., LIESA, C. L. & MAESTRO, A. 1999. Stress perturbations registered by jointing near strike-slip, normal, and reverse faults: examples from the Ebro Basin, Spain. *Journal of Geophysical Research* (B7) **104**, 15141–53.

SIMÓN, J. L. & SORIANO, M. A. 1985. Deformaciones cuaternarias en el area de Zaragoza. *Actas I Reunión de Cuaternario Ibérico* 329–343.

SIMÓN, J. L. & SORIANO, M. A. 1986. Diapiric deformations in the Quaternary deposits of the central Ebro basin, Spain. *Geological Magazine* **123**, 45–57.

SMITH, N. D. 1974. Sedimentology and bar formation in the upper kicking horse river, a braided outwash stream. *Journal of Geology* **82**, 205–23.

SMITH, G. A. 1986. Coarse-grained nonmarine volcaniclastic sediment: terminology and depositional processes. *Geological Society of America Bulletin* **97**, 1–10.

SOREGHAN, G. S., SOREGHAN, M. J., SWEET, D. E. & MOORE, K. D. 2009. Hot fan or cold outwash? Hypothesized proglacial deposition in the upper Paleozoic cutler formation, western tropical Pangea. *Journal of Sedimentary Research* **79**, 495–522.

SORIANO, M. A. 1990. *Geomorfología del sector centro-meridional de la Depresión del Ebro* 269 p. Ph.D. thesis, Instituto Fernando el Católico, Diputación Provincial de Zaragoza. Published thesis.

SORIANO, M. A., LUZÓN, A., YUSTE, A., POCOVÍ, A., PÉREZ, A., SIMÓN, J. L. & GIL, H. 2012. Quaternary alluvial sinkholes: record of environmental conditions of karst development, examples from the Ebro Basin, Spain. *Journal of Cave and Karst Studies* **74**, 173–85.

SORIANO, M. A. & SIMÓN, J. L. 1995. Alluvial dolines in the central Ebro Basin, Spain: a spatial and developmental hazard analysis. *Geomorphology* **11**, 295–309.

SORIANO, M. A. & SIMÓN, J. L. 2002. Subsidence rates and urban damages in alluvial dolines of the central Ebro Basin (NE Spain). *Environmental Geology* **42**, 476–84.

STEEL, R. J. & THOMPSON, D. B. 1983. Structures and textures in Triassic braided stream conglomerates ('Bunter' Pebble Beds) in the Sherwood Sandstone Group, N Staffordshire, England. *Sedimentology* **30**, 341–67.

SWEET, M. L. 1999. Interaction between aeolian, fluvial and playa environments in the Permian Upper Rotliegend Group, UK southern North Sea. *Sedimentology* **46**, 171–87.

TIRSGAARD, H. & ØXNEVAD, I. 1998. Preservation of pre-vegetational mixed fluvio-aeolian deposits in a humid climatic setting: an example from the Middle Proterozoic Eriksfjord Formation, Southwest Greenland. *Sedimentary Geology* **120**, 295–317.

VAN VLIET-LANÖE, B., MAGYARI, A. & MEILLIEZ, F. 2004. Distinguishing between tectonic and periglacial deformations of quaternary continental deposits in Europe. *Global and Planetary Change* **43**, 103–27.

VEIGA, G. D., SPALLETTI, L. A. & FLINT, A. 2002. Aeolian/fluvial interactions and high-resolution sequence stratigraphy of a non-marine lowstand wedge: the Avilé Member of the Agrio Formation (Lower Cretaceous), central Neuquén Basin, Argentina. *Sedimentology* **49**, 1001–19.

VENDEVILLE, B. C. & JACKSON, M. P. A. 1992. The rise of diapirs during thin-skinned extension. *Marine and Petroleum Geology* **9**, 331–53.

VISHER, G. S. 1969. Grain size distribution and depositional processes. *Journal of Sedimentary Petrology* **39**, 1074–106.

WALTHAM, T., BELL, F. & CULSHAW, M. 2005. *Sinkholes and Subsidence*. Chichester: Springer, 382 pp.